

# Strong UV and X-ray variability of the Narrow Line Seyfert 1 Galaxy WPVS 007 – on the nature of the X-ray low state

Dirk Grupe<sup>1</sup>, S. Komossa<sup>2</sup>, Julia Scharwächter<sup>3,4</sup>, Matthias Dietrich<sup>5,6</sup>, Karen M. Leighly<sup>7</sup>, Adrian Lucy<sup>7</sup>, Brad N. Barlow<sup>1</sup>,

## ABSTRACT

We report on multi-wavelength observations of the X-ray transient Narrow Line Seyfert 1 (NLS1) galaxy WPVS 007. The galaxy was monitored with *Swift* between October 2005 and July 2013, after it had undergone a dramatic drop in its X-ray flux earlier. For the first time, we are able to repeatedly detect this NLS1 in X-rays again. This increased number of detections in the last couple of years may suggest that the strong absorber that has been found in this AGN is starting to become leaky, and may eventually disappear. The X-ray spectra obtained for WPVS 007 are all consistent with a partial covering absorber model. A spectrum based on the data during the extreme low X-ray flux states shows that the absorption column density is of the order of  $4 \times 10^{23} \text{ cm}^{-2}$  with a covering fraction of 95%. WPVS 007 also displays one of the strongest UV variabilities seen in Narrow Line Seyfert 1s. The UV continuum variability anti-correlates with the optical/UV slope  $\alpha_{\text{UV}}$  which suggests that the variability primarily may be due to reddening. The UV variability time scales are consistent with moving dust ‘clouds’ located beyond the dust sublimation radius of  $R_{\text{sub}} \approx 20 \text{ ld}$ . We present for the first time near infrared JHK data of WPVS 007, which reveal a rich emission-line spectrum. Recent optical spectroscopy does not indicate significant variability in the broad and FeII emission lines, implying that the ionizing continuum seen by those gas clouds has not significantly changed over the last decades. All X-ray and UV observations are consistent with a scenario in which an evolving Broad Absorption Line (BAL) flow obscures the continuum emission. As such, WPVS 007 is an important target for our understanding of BAL flows in low-mass active galactic nuclei (AGN).

*Subject headings:* galaxies: active, galaxies: individual (WPVS 007)

<sup>1</sup>Department of Astronomy and Astrophysics, Pennsylvania State University, 525 Davey Lab, University Park, PA 16802; email: dxg35@psu.edu

<sup>2</sup>Max-Planck-Institut für Radioastronomie, Auf dem Hügel 69, 53121 Bonn, Germany

<sup>3</sup>Research School of Astronomy and Astrophysics, The Australian National University, Mount Stromlo Observatory, Cotter Road, Weston Creek, ACT 2611 Australia

<sup>4</sup>Observatoire de Paris, LERMA, 61 Avenue de l’Observatoire, F-75014 Paris, FRANCE, email: julia.scharwaechter@obspm.fr

<sup>5</sup>Department of Astronomy, The Ohio State University, 140 West 18th Avenue, Columbus, OH 43210, USA

<sup>6</sup>Dept. of Physics and Astronomy, Clippinger Labs 251B, Athens, OH 45701

<sup>7</sup>Homer L. Dodge Department of Physics and Astron-

## 1. Introduction

Outflows are a ubiquitous property of AGN. For example, blue-shifted emission lines like [OIII] $\lambda$ 5007 (e.g., Komossa et al. 2008a), or blue shifted absorption lines in the UV and in X-rays (e.g., Crenshaw et al. 2004) are typically interpreted as signs of outflowing gas. Outflows can be driven in principle magnetically, thermally, and through radiation (e.g., Kurasawa & Proga 2009a,b; Proga & Kallman 2004). With the kinetic energy and angular momentum transported outwards, outflows have strong influences on the

omy, University of Oklahoma, 440 West Brooks Street, Norman, OK 73019; email: leighly@nhn.ou.edu

AGN environment. As a consequence, many AGN parameters are driven by the Eddington ratio  $L/L_{\text{Edd}}$  (e.g., Boroson 2002; Sulentic et al. 2000; Grupe 2004; Xu et al. 2012). The class of AGN that shows the strongest outflows (besides jets) are Broad Absorption Line Quasars (BAL QSOs, e.g., Weymann et al. 1991) which can reach outflow velocities of more than 20000 km s<sup>-1</sup> (e.g., Hamann et al. 2008). Roughly 10-20% of optically-selected quasars belong to this class (e.g., Dai et al. 2008; Elvis 2000) with increasing percentage among infrared selected samples, which is often interpreted as an inclination effect. However, it has also been suggested that the occurrence of BALs may mark a specific time in the life of a quasar (Mathur 2000; Becker et al. 2000). Because the strength of radiation driven outflows directly depends on  $L/L_{\text{Edd}}$ , BAL QSOs are at one extreme end of the  $L/L_{\text{Edd}}$  distribution (e.g., Boroson 2002). In the local Universe the AGN with the highest  $L/L_{\text{Edd}}$  are Narrow Line Seyfert 1 galaxies (NLS1s; Osterbrock & Pogge 1985).

NLS1s have drawn a lot of attention over the last two decades due to their extreme properties, such as, on average, steep X-ray spectra, strong Fe II emission and weak emission from the Narrow Line Region (e.g., Boroson & Green 1992; Grupe 2004; Komossa 2008). All these properties are linked, and are most likely driven primarily by the mass of the central black hole and the Eddington ratio  $L/L_{\text{Edd}}$ . Generally speaking, NLS1s are AGN with low black hole masses and high  $L/L_{\text{Edd}}$ . NLS1s have also been considered to be AGN in an early stage of their evolution (Grupe et al. 1999; Mathur 2000).

It has been suggested by Brandt & Gallagher (2000) and Boroson (2002) that BAL QSOs and NLS1s are similar with respect to their high  $L/L_{\text{Edd}}$ . However, they differ in their black hole masses and appear to be at opposite ends of the  $M_{\text{BH}}$  spectrum. It has also been found that the rest-frame optical spectra of at least some BAL QSOs look very much like low-redshift NLS1s (e.g., Marziani et al. 2009; Dietrich et al. 2009). While all these results seem to support the connection between BAL QSO and NLS1s, what is missing is a direct link between them: an AGN that shows properties of a typical NLS1 as well as those of BAL QSOs. Such a link is the NLS1 WPVS 007.

When the NLS1 WPVS 007 (RBS 0088; 1RXS J003916.6–511701;  $\alpha_{2000} = 00^{\text{h}}39^{\text{m}}15.^{\text{s}}8$ ,  $\delta_{2000} = -51^{\circ}17'03''0$ ,  $z=0.02861$ ; Wamsteker et al. 1985; Grupe et al. 1995; Schwobe et al. 2000) was discovered in X-rays during the ROSAT All Sky Survey (RASS; Voges et al. 1999) it appeared to be a normal X-ray bright AGN, although its X-ray spectrum was unusually soft (Grupe et al. 1995). However, when it was observed again three years later with the ROSAT Position Sensitive Proportional Counter (PSPC; Pfeffermann et al. 1986) it appeared to have almost vanished in X-rays, with a factor of more than 400 drop in its X-ray flux (Grupe et al. 1995). In the following years it was observed several times by ROSAT (Grupe et al. 1995) and Chandra in 2002 (Vaughan et al. 2004). During all these observations, WPVS 007 was extremely X-ray faint. We started monitoring WPVS 007 with the NASA Gamma-Ray Burst Explorer mission *Swift* (Gehrels et al. 2004) in October 2005 (Grupe et al. 2007a) and were able to finally detect it with *Swift* in a 50 ks observation in September 2007 (Grupe et al. 2008b). This observation led to the detection of hard X-ray photons in the X-ray spectrum of WPVS 007 for the first time. The hard X-ray spectrum suggested the presence of a strong partial covering absorber.

The strongest clue that the X-ray transience is due to absorption, however, came from UV spectroscopy. In 1996, WPVS 007 was observed by HST (Goodrich 2000) and low-velocity broad absorption troughs (mini BALs) were present in the UV resonance lines. As suggested by Hamann et al. (2008) mini BALs may be the early (or late) states of BALs. When WPVS 007 was observed again in the UV by FUSE in 2003 it had developed a very strong broad absorption line flow (Leighly et al. 2009). HST COS UV spectra obtained in 2010 June showed a dramatic increase in the UV SiIV and CIV absorption lines (Cooper et al. 2013) compared with the 1996 HST observation.

WPVS 007 is special because BALs are rare in such low-luminosity systems as WPVS 007 (e.g., Laor & Brandt 2002), and because it allows us to study properties which otherwise can not be studied easily in BAL QSOs. Due to their large black hole masses, the time scales observed in BAL QSOs are very long, and at least on the order

of years (e.g., Capellupo et al. 2011; Saez et al. 2012). In WPVS 007, however, time scales are shorter, as it is 100 times less luminous than a typical BALQSO and with a similarly smaller black hole mass and typical size scales (Leighly et al. 2009).

The outline of this paper is as follows: in §2 we describe the observations by *Swift*, in the near infrared, and in the optical, as well as the data reduction. In §3 we present the results from the analysis of the light curves and X-ray spectroscopy of the *Swift* XRT data and the optical and near infrared spectroscopy. In §4 we discuss the results. Throughout the paper spectral indices are denoted as energy spectral indices with  $F_\nu \propto \nu^{-\alpha}$ . Luminosities are calculated assuming a  $\Lambda$ CDM cosmology with  $\Omega_M=0.27$ ,  $\Omega_\Lambda=0.73$  and a Hubble constant of  $H_0=75$  km s $^{-1}$  Mpc $^{-1}$ . This results in a luminosity distances  $D=118$  Mpc using the cosmology calculator by Wright (2006). All errors are  $1\sigma$  unless stated otherwise.

## 2. Observations and data reduction

### 2.1. *Swift* Observations

Table 1 presents the *Swift* observations of WPVS 007 starting on 2008 January 15, including the start and end times and the total exposure times. The lists of the previous *Swift* observations between 2005 October and 2007 December can be found in Grupe et al. (2007a) and Grupe et al. (2008b). The *Swift* X-ray telescope (XRT; Burrows et al. 2005) was operating in photon counting mode (Hill et al. 2004) and the data were reduced by the task *xrtpipeline* version 0.12.6., which is included in the HEASOFT package 6.12. Source counts were selected in a circle with a radius of 24.8'' and background counts in a nearby circular region with a radius of 247.5''. The  $3\sigma$  upper limits and the count rates of the detections were determined by applying the Bayesian method by Kraft et al. (1991). For these detections, due to the low number of counts, we applied Bayesian statistics to determine the hardness ratios as described by Park et al. (2006). Some of the detections allowed a spectral analysis using Cash statistics (Cash 1979). In some cases, like in the already published observation from September 2007, the data from several segments when WPVS 007 was detected were merged.

For this purpose we created auxiliary response files (ARF) for each segment and then combined these into one arf by using the FTOOL *addarf*. For all spectra we used the most recent response file *swxpc0to12s6\_20010101v013.rmf*. Due to the small number of counts used in the spectra, the counts were not binned.

The UV-optical telescope (UVOT; Roming et al. 2005) data of each segment were coadded in each filter with the UVOT task *wotimsum*. Source counts in all 6 UVOT filters were selected in a circle with a radius of 5'' and background counts in a nearby source free region with a radius of 20''. UVOT magnitudes and fluxes were measured with the task *wotsource* based on the most recent UVOT calibration as described in Poole et al. (2008) and Breeveld et al. (2010). The UVOT data were corrected for Galactic reddening ( $E_{B-V} = 0.012$ ; Schlegel et al. 1998). The correction factor in each filter was calculated with equation (2) in Roming et al. (2009) who used the standard reddening correction curves by Cardelli et al. (1989). Due to new UVOT calibration files (Breeveld et al. 2010) also observations that were previously published in Grupe et al. (2007a) and Grupe et al. (2008b) were reanalyzed in order to have a consistent data set. All these UVOT data starting in October 2005 are listed with their magnitudes corrected for Galactic reddening and the optical/UV spectral slope  $\alpha_{UV}$  in Table 2. This optical/UV spectral slope  $\alpha_{UV}$  was determined from a power law fit to the UVOT data. Note that although we generally observed WPVS 007 with the *Swift* UVOT in all 6 filters since the beginning of the monitoring campaign in 2005, we switched to the uv m2 filter only after the end of the *Swift* guest investigator program in March 2012 in order to save on UVOT filter wheel rotations. The uv m2 filter was picked because it is the cleanest UV filter with no broad wings in the filter response (Breeveld et al. 2010).

In order to obtain spectral energy distributions, a source and background spectral file was created for each filter using the UVOT task *wot2pha*. Also here the latest UVOT response files for each filter were used.

#### 2.1.1. Near Infrared (NIR) Observations

We observed WPVS 007 as part of an observing program using the NIR imaging spectro-

graph Soff at the 3.5 m NTT at La Silla/ESO, to study the rest-frame optical spectra of a sample of BAL QSOs (Dietrich et al. 2009). The observation was performed on 2004 September 12 (MJD 53260.112) for  $18 \times 180$ s in the J plus H, and  $8 \times 180$ s in the H plus K band wavelength ranges under photometric conditions with  $1''$  seeing. A  $1''$  long slit was used for the observation. We used an  $1024 \times 1024$  pixel<sup>2</sup> Rockwell HAWAII HgCdTe detector. The data were reduced with ESO’s Munich Imaging and Data Analysis System, MIDAS. The data reduction was carried out the same way as in Dietrich et al. (2009), and a full description can be found in that work.

### 2.1.2. Optical Spectroscopy

An optical spectrum of WPVS 007 was obtained on 30 September 2011 using the Wide Field Spectrograph WiFeS (Dopita et al. 2007, 2010) at the ANU 2.3m telescope at Siding Spring Observatory (Australia). WiFeS is an integral field spectrograph with a field of view of  $38'' \times 25''$  produced by 25 slitlets of  $38'' \times 1''$ . The instrument provides a wide wavelength coverage via simultaneous observations in a blue and red arm at spectral resolutions of 3000 or 7000. WPVS 007 was observed using the B3000 grating in the blue arm and the R7000 grating in the red arm. The data presented here are the median average of five exposures of 600 s each. The observations were performed in nod-and-shuffle mode for sky-subtraction, using 100 s integrations on the object and the sky. A bias frame and a Ne-Ar lamp exposure were taken between the object exposures in order to be able to account for variations in the bias level and the wavelength solution during the night. The data reduction is based on the reduction recipes implemented in the IRAF reduction package for WiFeS (see Dopita et al. 2010). A B4V star, observed shortly before WPVS 007, is used as a template star for correcting telluric features in the red part of the spectrum. The spectrophotometric calibration is based on observations of CD-30 18140 obtained during the same observing night. Since the night was partly cloudy, the absolute flux calibration is uncertain. In this paper, we present the integrated nuclear spectrum of WPVS 007 obtained for a spatial aperture of 1 arcsec.

On 23 October 2012, we obtained multiple spectra of WPVS 007 with a total integration time of

1800 s using the Goodman High Throughput Spectrograph on the 4.1-m SOUTHERN Astrophysical Research (SOAR) telescope (Clemens et al. 2004). We used the  $0''.84$  long slit in conjunction with the 930 1/mm VPH grating, which has a dispersion of 0.417  $\mu\text{m}$  per unbinned pixel. This setup allowed us to cover the spectral range 4130-5830  $\text{\AA}$  with a resolution of 2.3  $\text{\AA}$  ( $R=2100$ ); the mean signal-to-noise ratio in the combined spectrum was approximately 110 per resolution element. Standard IRAF routines were used to bias-subtract, flat-field, and wavelength-calibrate (using FeAr lamp spectra) the spectral frames. Flux calibration was achieved using observations of the spectrophotometric standard star LTT 3218 (spectral type: DA) obtained using the same instrumental configuration as WPVS 007.

## 3. Results

### 3.1. X-ray Variability

Table 4 lists the *Swift* detections of WPVS 007. The *Swift* X-ray light curve with these detections is displayed in Figure 1 which also shows the light curves in each of the 6 UVOT filters. The first detection of WPVS 007 by *Swift* was obtained in 2007 September when *Swift* collected more than 50 ks of data on the source (Grupe et al. 2008b). The X-ray light curve of the top panel of Figure 1 also shows the count rates determined from the data when WPVS 007 is not detected in a single observation with the *Swift* XRT. These data points are displayed as red crosses. The entire long-term X-ray 0.2-2.0 keV flux light curve starting with the discovery during the RASS is displayed in Figure 2.

The strongest *Swift* detection was found on 2009 September 17 when WPVS 007 was at a level of  $1.6 \times 10^{-15} \text{ W m}^{-2}$  (equivalent to  $1.6 \times 10^{-12} \text{ erg s}^{-1} \text{ cm}^{-2}$ ) which was just a factor of 3.5 fainter than during the detection during the RASS. This ‘high state’ however, lasted only for a few days.

When we observed WPVS 007 again with *Swift* a week later in a ToO observation, we did not detect the AGN anymore. The  $3\sigma$  upper limit at the position of WPVS 007 was  $2.3 \times 10^{-3} \text{ counts s}^{-1}$  which converts to  $2.0 \times 10^{-16} \text{ W m}^{-2}$  assuming the spectrum of the 2009 September 17 (MJD 55091) observation.

We note that Figure 2 only displays the X-



ray detections of WPVS 007, except for two upper limits in the ROSAT HRI. However, typically WPVS 007 is not detected by the *Swift* XRT in the 2 or 5 ks monitoring observations. The detection limit for a 5ks *Swift* XRT observation is of the order of  $1 \times 10^{-3}$  counts  $s^{-1}$  and the  $3\sigma$  upper limit for a 2 ks observation is of the order of  $3 \times 10^{-3}$  counts  $s^{-1}$ . The *Swift* XRT  $3\sigma$  upper limits are listed in Table 3 and displayed together with the XRT detections in Figure 3. This figure clarifies that most of the time WPVS 007 is un-detectable by *Swift* and that WPVS 007 is typically at a count rate below about  $1 \times 10^{-3}$  counts  $s^{-1}$ . Note that the  $3\sigma$  upper limits during the first two years of our monitoring program from 2005 and 2006 (target ID 30334, segments 001 to 013) have been previously published in Grupe et al. (2007a).

The increased number of detections especially during our intensive monitoring campaign in 2011 September (2011-September-01 = MJD 55805), as shown in the right panel of Figure 4, may suggest that the strong absorber that is most likely the cause for the X-ray weakness of WPVS 007 has started to disappear. It is worth noting that during the intensive monitoring campaign in 2010 June (2010-June-02 = MJD 55349) we only got two marginal detections (left panel of Figure 4).

In order to check the assumption that WPVS 007 has generally become brighter over the last decade, we co-added data over long periods which are displayed as red points in the XRT count rate light curve in Figure 1. These data points suggest that WPVS 007 has indeed become brighter between 2005 and about 2009, however, our recent *Swift* observations during the intense monitoring campaign in September 2011 and thereafter indicate that this trend did not persist, and instead, the AGN has become fainter again. Adding all data between 2011 October and 2013 July (total exposure time 82 ks) results in a  $3\sigma$  detection at a level of  $2.46^{+2.42}_{-1.71} \times 10^{-4}$  counts  $s^{-1}$ .

The X-ray detections of WPVS 007 over the last years not only show strong flux variability, but the hardness ratios listed in Table 4 suggest strong spectral variability as well. While during the 'low-state' during the 2007 September observation WPVS 007 appeared to be very hard with a hardness ratio  $HR = +0.54^{+0.18}_{-0.12}$ , during the 'high state' in 2009 September 17 the hardness ratio was very soft with  $HR = -0.54^{+0.13}_{-0.16}$ . Such behavior

may be expected from a partial covering absorber. While hardness ratios can give some spectral information, a spectral analysis of the data is required to see if the data are consistent with a partial covering absorber model (see below).

### 3.2. X-ray spectral analysis

As shown in Section 3.1, WPVS 007 is not detected typically in a single 5ks observation. In order to obtain spectra, the data of several observations have to be combined. This method was applied to derive the photon distribution shown in Grupe et al. (2008b) from the *Swift* XRT observations in 2007 September. These data were consistent with a neutral partial covering absorber model with an absorption column density of  $N_{\text{H}} = 1 \times 10^{23}$   $\text{cm}^{-2}$  and a covering fraction  $f_{\text{pc}} = 0.95$ .

Table 5 lists the spectral analysis for detections when more than 30 source counts were detected in a single observation. Due to the low number of counts in the single detections during the intense daily monitoring campaign in 2011 September, we combined the data into one spectrum. Although the number of counts even during the brightest X-ray detections are low it still allows a limited spectral analysis using Cash statistics (Cash 1979). The analysis of these spectra confirms the strong spectral variability found from the hardness ratios listed in Table 4. While the data of 2009 September 17, and 2010 July 13, are both consistent with a single power law model with a relatively flat X-ray spectral slope  $\alpha_{\text{X}}=1.6$  all other data require a partial covering absorber model. An F-test between the power law and partial covering absorber models of the 2007 September and 2011 July data shows that there is a 1% chance that the data are drawn from a random distribution. This is, however, not the case for the 2011 September data which clearly require a partial covering absorber model with  $N_{\text{H,pc}} = 8.45^{+5.65}_{-2.40} \times 10^{22}$   $\text{cm}^{-2}$ . Here the probability of a random result is 0.3%.

The spectral analysis of all these spectra was based on data when WPVS 007 was in relatively high X-ray flux states. This may not represent the data when WPVS 007 is below the detection threshold. In order to determine the spectrum in these very low X-ray flux states, we combined all data when only  $3\sigma$  upper limits could be measured during the observations listed in Table 3. We merged all these data from 2005 October to 2013

July and obtained a source plus background spectrum with 267 counts with a total exposure time of 434 ks. These data were binned with 15 counts per bin (noted as 2005-2013 in Table 5). Clearly, as expected, the single power law model does not fit the data. We fitted the spectrum with a partial covering absorber model and found a high column density of  $N_{\text{H}} = 3.6 \times 10^{23} \text{ cm}^{-2}$  (Table 5). This absorption column density is significantly higher than during the times when WPVS 007 is detected by the *Swift* XRT, suggesting that at least in part the strong X-ray variability that we see in this AGN is indeed caused by a change in the absorber column density.

A fit with the ionized partial covering absorber model *zxipcf* (Reeves et al. 2008) suggests an absorber column density of the order of  $2 \times 10^{23} \text{ cm}^{-2}$  with an ionization parameter of the order of  $\xi \approx 1$  and a covering fraction of 0.96. These values (in particular, the column density) agree roughly with the values derived from Cloudy modeling of the absorption lines in the 2003 FUSE spectrum Leighly et al. (2009). Note, however, that due to the low number of counts these values are not well constrained at all.

### 3.3. UVOT data

Figure 1 displays the complete UVOT light curves in all 6 filters since the beginning of the *Swift* monitoring campaign in October 2005. The light curves during the two intensive monitoring periods in 2010 June and 2011 September are displayed in Figure 4. All magnitudes are listed in Table 2. These data show that WPVS 007 is one of the most UV variable NLS1s besides Mkn 335 which has shown even larger amplitude variations (Grupe et al. 2012). Typically NLS1s seem to vary by about 0.3 mag in the UV (Grupe et al. 2010). *Swift* has monitored several AGN, especially NLS1s, over long time scales, such as CBS 126, PG 1211+143, or PKS 0558-504 (Chiang et al. 2012; Bachev et al. 2009; Gliozzi et al. 2010, 2012, respectively) but none of these has shown the amplitude of variability as observed in Mkn 335 and WPVS 007. The maximum amplitude of variability seen in WPVS 007 was 0.66 mag in W2 within a month between 2008 June 19 and October 21 (MJDs 54636-54760), and 0.53 mag within two months between 2010 November 20 and 2011 January 19. Figure 9

displays the optical/UV luminosities in all six UVOT filters during these observations. Clearly, not only has the AGN become brighter during the 2011 January 19 observation, but also the UV spectral slope  $\alpha_{\text{UV}}$  has become bluer from  $\alpha_{\text{UV}}=1.00\pm 0.05$  during the 2010 November 20 observation to  $\alpha_{\text{UV}}=0.72\pm 0.09$  in the January 2011 observation. WPVS 007 varies on timescales of days. As displayed in Figure 4 when we performed daily monitoring campaigns of WPVS 007 in June 2010 and September 2011, the UV flux/magnitude changes significantly within a few days.

Note that host galaxy contamination is an issue in low-luminosity AGN such as WPVS 007. In Grupe et al. (2010) we discussed a method to test the significance of the host galaxy contribution by extracting the UVOT data using different source extraction radii. Using the standard 5'' extraction radius and a 3'' extraction radius (including the parameter `apercorr=curveofgrowth` in `uvotsource`) results in a difference of 0.15 mag in V and 0.05 mag in W2. What this means is that we do overestimate the brightness in V slightly, but in W2 the effect of host galaxy contamination is negligible. The effect on spectral slopes such as  $\alpha_{\text{ox}}$  and  $\alpha_{\text{UV}}$  is negligible because these are dominated by UV emission where host galaxy contribution is very low.

Figure 5 shows the flux measured in the UVOT M2 filter vs. the optical/UV slope  $\alpha_{\text{UV}}$ . There is a clear anti-correlation between these two properties. The AGN becomes redder with decreasing UV flux. A Spearman rank order correlation analysis results in  $r_s=-0.76$  (116 data points),  $T_s=-12.56$  with a probability  $P < 10^{-8}$  of a random result. Figure 6 displays the relation between the magnitude in the UVOT W2 filter<sup>1</sup> and the XRT count rate during a detection as listed in Table 4. We do not find any clear correlation between these two properties. There is only a light trend that the source appears to be brighter in the UV when it is fainter in X-ray. However, this trend is not statistically significant.

The monitoring in all 6 UVOT filters over 6 years allows to check for any time delays between different band passes. We applied cross-correlation analysis to the data in particular the

<sup>1</sup>The UVOT W2 filter was picked here because it is the bluest filter which is closer to the X-ray emission

data during the daily monitoring campaigns in June 2010 and September 2011. We did not find any significant delays between the light curves. The detections in X-rays, however, are too sparse to allow for any cross correlation analysis between the X-ray and UVOT light curves.

### 3.4. Spectral Energy Distribution

With several X-ray detections of WPVS 007 we are able to study the variability of the spectral energy distribution (SED). Figure 7 displays the SEDs during the 2009 September 17 ‘high state’ and the ‘low state’ observations during the 2010 June 10 *Chandra* observation<sup>2</sup> and the 2011 September (combined data) *Swift* detection. In addition this plot also made use of near infrared data from the Two Micron All Sky Survey (2MASS) and mid-infrared data from the Wide-field Infrared Survey Explorer (WISE). The fluxes and luminosities of the 2MASS and WISE measurements are listed in Table 6.

All optical to X-ray spectral slopes  $\alpha_{\text{ox}}$  for each X-ray detection of WPVS 007 are listed in Table 4<sup>3</sup>. During the *Chandra* observation on 2010 June 10 and the *Swift* detection in 2011 September the optical to X-ray spectral slope  $\alpha_{\text{ox}}$ <sup>4</sup> was 2.49. Following the definition by Brandt et al. (2000), at those times WPVS 007 was an X-ray weak AGN. During the 2009 September 17 ‘high state’, however, the slope was  $\alpha_{\text{ox}}=1.89$ . This value is still significantly larger than expected from a low-luminosity AGN such as WPVS 007. According to the  $\alpha_{\text{ox}}-\log l_{2500\text{\AA}}$  relation given in Grupe et al. (2010) (equation 12) we would have expected the optical to X-ray spectral slope to be about  $\alpha_{\text{ox}}=1.26$ . This is the same value that can be derived from the relation given by Just et al. (2007) and Strateva et al. (2005). Even when corrected for absorption, WPVS 007 still remains rather X-ray quiet considering its UV luminosity density. The changes in the optical to X-ray spectral slopes  $\alpha_{\text{ox}}$  become apparent when looking at

Figure 7. These changes are primarily driven by the strong changes in the X-ray spectra. Note that there is no correlation between the optical-to-X-ray spectral slope  $\alpha_{\text{ox}}$  and the UV spectral slope  $\alpha_{\text{UV}}$ . In general, there is a strong anti-correlation between  $\alpha_{\text{ox}}$  and  $\alpha_{\text{UV}}$  found among AGN as shown from the *Swift* observations by Grupe et al. (2010). However, all optical-to-X-ray spectral slopes measured for WPVS 007 are outside the  $\alpha_{\text{ox}}$  range shown in Grupe et al. (2010). From its  $\alpha_{\text{UV}}$  of the order of +0.80 one would expect the  $\alpha_{\text{ox}}$  to be about 1.3, which is obviously not the case.

In Grupe et al. (2010) we fitted optical to X-ray part of the SEDs with a power law with exponential cutoff model to represent the UV/EUV part of the spectrum and an absorbed power law model in the X-ray regime. However, although this model can describe the data, it is not a physical model and in some cases leads to overestimating the bolometric luminosity. Recently Done et al. (2012) introduced a spectral fit model *optxagnf* which models the spectrum of a thin accretion disk including a color correction of the blackbody component, comptonization in the disk to obtain the soft X-ray excess, and inverse Compton up-scattering to form the hard X-ray component. This model is included in the most recent version of *XSPEC* 12.7.1.

We applied this model to the 2009 September 17 ‘high state’ data. Due to the low number of X-ray counts in that observation we can use this model only for a consistency check. We measured a bolometric luminosity of  $\log L_{\text{bol}} = 6 \times 10^{37}$  W (equivalent to  $6 \times 10^{44}$  erg s<sup>-1</sup>). With its black hole mass of  $4 \times 10^6 M_{\odot}$  (Leighly et al. 2009) this means that WPVS 007 is accreting at the Eddington limit. Note, that this is a factor of 10 higher than what was estimated by Leighly et al. (2009) based on the 1996 HST FOS spectrum. However, this is consistent with the long-term X-ray light curve shown in Figure 2.

### 3.5. Near Infrared Spectroscopy

Figure 8 displays the 2004 NTT SOFI NIR spectrum of WPVS 007 in the J plus H and H plus K bands. It is rich in emission lines. Transitions were identified following the NIR spectra of NLS1s published by Landt et al. (2008); Garcia-Rissmann et al. (2012) and the line catalogue of the National Institute of Standards

<sup>2</sup>The full analysis of the *Chandra* data will be presented in Cooper et al. (in prep.)

<sup>3</sup>Except for the 2007 September observation when the *Swift* UVOT was still turned off during the gyro recovery phase (See Grupe et al. 2008b, for details)

<sup>4</sup> $\alpha_{\text{ox}} = -0.384 \log(f_{2\text{keV}}/f_{2500\text{\AA}})$  as defined by Tananbaum et al. (1979). The uncertainties in  $\alpha_{\text{ox}}$  are 0.2

(NIST, Ralchenko et al. 2011). As pointed out by Landt et al. (2008), NIR spectroscopy of Seyfert 1 galaxies is a relatively new field and only some brighter AGN have been studied in the NIR (e.g., Rodriguez-Ardila et al. 2011; Grupe & Thomas 2002). WPVS 007 exhibits very strong FeII and FeI emission lines, even stronger than in the NLS1 prototype I Zw 1 (see Garcia-Rissmann et al. 2012). All identified emission lines in the NIR spectra are listed in Table 7 with their Full Width at Half Maximum (FWHM) and line flux. The equivalent widths of the Pa $\alpha$  and Br $\gamma$  lines are 68 and 7.6 $\text{\AA}$ , respectively. Compared with other NLS1s, as, e.g., listed in Grupe & Thomas (2002), these values appear to be at the higher end.

### 3.6. Optical spectroscopy

Figure 10 displays the most recent optical spectra obtained for WPVS 007 at the 2.3m ANU telescope in September 2011, and the 4.1m SOAR telescope on Cerro Pachon in Chile in October 2012 (left and right panels, respectively). The reason for taking these optical spectra was to see, whether any changes in the emission lines had occurred (since the 1990s), given the strong apparent changes of observed (line-of-sight) continuum emission (note that FeII variability has been reported previously by, e.g., Giannuzzo & Stirpe (1996) and Shapovalova et al. (2012)).

For the 2011 September spectrum, which was taken with the Integrated Field Spectrograph, we extracted a nuclear spectrum with 1" extraction radius. We do not find significant changes in the FeII fluxes over more than a decade. Spectra taken in 2007 at CTIO (Dunn et al. 2008), and most recently with the 4.1m SOAR telescope, confirm that there are no significant changes in the emission line strengths compared with the spectra taken in 1992 and 1995 (the properties of the optical emission lines measured at that time were given in Grupe et al. (1999)). This result then implies that no dramatic changes have occurred in the photoionizing continuum seen by the Balmer-line emitting gas

## 4. Discussion

### 4.1. On the nature of the X-ray low-state of WPVS 007

We presented new *Swift* observations on the X-ray transient NLS1 WPVS 007 covering a period between October 2005 (Grupe et al. 2007a, 2008b) and March 2013, in order to see whether the X-ray faintness of WPVS 007 persisted, or whether, and in which way, the source re-brightened again. We find, that WPVS 007 remains below the *Swift* detection limit most of the time, but shows some periods of short-term fluctuations in X-ray flux, increasing almost to the initial ROSAT high-state once in 2009.

A key question then concerns the nature of the X-ray faintness of WPVS 007: is its X-ray weakness intrinsic, or caused by absorption along the line of sight and related to the strong UV BAL flow which developed in the UV? What causes the short-timescale high-amplitude fluctuations we see with *Swift*?

We begin with a short summary of X-ray weak AGN and models suggested to explain them, and then move on to exploring the link between the long-lasting X-ray low-state of WPVS 007 and its strong UV BALs.

While NLS1s as a population typically appear to be bright in X-rays, their high  $L/L_{\text{Edd}}$  and steep X-ray spectral slope  $\alpha_X$  result in a steeper optical-to-X-ray spectral slope  $\alpha_{\text{ox}}$ , which makes them appear to be X-ray weaker when compared with Broad Line Seyfert 1s (e.g., Grupe et al. 2010) when comparing the X-ray to the UV flux. However, generally speaking they do not appear to be X-ray weak according to the definition of X-ray weakness of  $\alpha_{\text{ox}} > 2.0$  as given by Brandt et al. (2000). Nevertheless X-ray weak NLS1s are known (e.g., Williams et al. 2002, 2004). Among the best-studied examples are PHL 1811 (Leighly et al. 2007a) and PHL 1092 (Gallo et al. 2004; Miniutti et al. 2012). X-ray weak quasars have even been reported at high redshifts (Wu et al. 2011). Therefore, X-ray weakness may not be so uncommon even among NLS1s.

Recently Miniutti et al. (2012) reported a drop in the soft X-ray flux in PHL 1092 by a factor of 260 between 2003 and 2008. This is a drop in X-ray flux similar to WPVS 007. PHL 1811 has



an  $\alpha_{\text{ox}}=2.3$  (Leighly et al. 2007a) which is similar to WPVS 007 when detected. PHL 1092 displays variability in the X-ray loudness between  $\alpha_{\text{ox}}=1.6$  and 2.5 (Miniutti et al. 2012), which again is similar to the variability in  $\alpha_{\text{ox}}$  we have found in WPVS 007 (see Table 4). X-ray variability in other AGN, and NLS1 galaxies in particular, of much lower amplitude has typically been interpreted in terms of either absorption or reflection, or both. Example seen by *XMM-Newton* as well as *Suzaku* are: PG 2112+059 (Schartel et al. 2010), PG 0844+349 (Gallo et al. 2011), MCG-6-30-15 Inoue et al. (2011), NGC 4051 (Lobban et al. 2011), Mkn 335 (Grupe et al. 2012), Fairall 9 Lohfink et al. (2012), 1H0707-495 (Miller et al. 2010; Fabian et al. 2012; Dauser et al. 2012), and RX J2340-5329 (Schartel et al. 2013).

However, WPVS 007 is different from all these X-ray weak AGN and absorbed AGN. As discussed by Leighly et al. (2007a) for PHL 1811, the X-ray spectrum of this NLS1 can be fitted by a single power law with just Galactic absorption with no evidence for an intrinsic absorber in the line of sight. This, however, is not the case in WPVS 007. Its X-ray spectra can simply not be fit by a single power law model.

We also note that none of the X-ray weak NLS1 galaxies, including PHL 1092 and PHL 1811, do show any signs of UV absorption lines (Leighly et al. 2007a; Leighly et al. 2007b). As we know, this is certainly not the case in WPVS 007 where strong, deep BAL troughs have been found (Leighly et al. 2009). The detection of these strong BAL troughs in the UV therefore strongly suggests that the deep and long-lasting X-ray low-state of WPVS 007 is caused by absorption. Fluctuations in the X-ray count rate could then be caused by clumpiness of this absorber as it crosses the line of sight<sup>5</sup>

We have shown that the fits to the X-ray data of WPVS 007 significantly improve when a partial covering absorber model is applied instead of a single power law model (see Table 5)<sup>6</sup>. A

<sup>5</sup> Note that although variable BALs are common, the transitional change as observed in WPVS 007 is extremely rare (e.g., Hamann et al. 2008; Capellupo et al. 2011; Filiz Ak et al. 2012).

<sup>6</sup>In general, the curvature found in X-ray spectra, such as seen here in WPVS 007, can also be modeled by a blurred reflection model; as we have demonstrated for the

large absorption column density of about  $5 \times 10^{23} \text{ cm}^{-2}$  is inferred, when the AGN is not detectable in single *Swift* XRT observations. During times when WPVS 007 is detected, the absorption column density is significantly lower (see Table 5). To summarize, the X-ray variability observed in WPVS 007 is consistent with a variable partial covering absorber in the line of sight.

The column density of the absorber, inferred from UV observations, is on the order of  $2 \times 10^{23} \text{ cm}^{-2}$ , with a photoionization parameter  $\xi$  of the order of 1, assuming solar metallicity. Since the UV absorber is ionized, and in order to compare more directly with the X-rays, we have re-fitted the *Swift* data derived from the observations when WPVS 007 was not detected with the *ionized* partial covering absorber model *zxipcf* (Reeves et al. 2008). We find that the absorption column density and ionization parameter derived from this spectrum agrees with the 2003 FUSE data. Deep *simultaneous* UV and X-ray spectroscopy observations would be required, however, in order to perform a more rigorous comparison.

#### 4.2. UV variability

As shown in the *Swift* UVOT light curve (Figures 1 and 4), WPVS 007 varies strongly in the UV on long as well as intermediate time scales.

As for the optical/UV we noticed a strong anticorrelation between the flux measured in the UV (M2 filter) and the optical/UV spectral slope  $\alpha_{\text{UV}}$ . There are several ways to explain such an anticorrelation. For instance, (a) intrinsically by a change in the accretion rate and therefore  $L/L_{\text{Edd}}$ , or (b) by a change in the reddening. As shown by Grupe et al. (2010), there is a clear correlation between the Eddington ratio  $L/L_{\text{Edd}}$  and the UV spectral slope  $\alpha_{\text{UV}}$ . If we estimate  $L/L_{\text{Edd}}$  based on the extreme values of  $\alpha_{\text{UV}}$  of about 1.1 and 0.7 we find  $L/L_{\text{Edd}}$  ratios of 0.54 and 0.95, respectively. Alternatively, to cause a change in the optical/UV continuum as shown in Figure 9 only requires a change in the intrinsic  $E_{\text{B-V}}$  by 0.06 mag. We note in passing that the UV absorption lines are outside the wavelength windows of the UVOT filters, and so we are insensitive to any

X-ray faint and intermediate states in the NLS1 Mkn 335 (Grupe et al. 2007b, 2008a, 2012; Gallo et al. 2013). Mkn 335, however, lacks strong UV absorption features.

changes in the UV absorption lines.

Dusty clouds in motion, passing our line-of-sight, may therefore be responsible for the observed UV variability. Dust does not survive temperatures higher than 1500K. The dust sublimation radius (of a dusty medium around the central black hole) can be estimated by the relation given in, e.g., Kishimoto et al. (2011) with  $R_{\text{sub}} = 0.47 \times (6 \times \nu L_{5500\text{\AA}})^{0.5}$  where  $L_{5500\text{\AA}}$  is the luminosity at 5500Å in units of  $10^{39}$  W and  $R_{\text{sub}}$  the dust sublimation radius in units of pc. Using the optical spectra of WPVS 007 we can estimate the inner radius of the torus of the order of about 20 light days.

If we assume that WPVS 007 is similar in structure to a BAL QSO, then the wind of WPVS 007 has two components, a gaseous, dust free component that is responsible for the absorption in X-rays and the UV broad absorption lines, and a dusty component which is at larger radii with  $R > R_{\text{sub}} 20 \text{ ld}$  (0.05 pc). The broad line region gas on the other hand in WPVS 007 is located at  $R_{\text{BLR}} = 5 \text{ ld}$  following the relation by Kaspi et al. (2000). This is significantly smaller than the dust sublimation radius. (This, then, of course, can explain why we do see significant variability in the UV continuum, caused by dust, without affecting the photoionizing continuum that is seen by the BLR.)

At a distance of 20 ld, the velocity of the dust cloud around the central black hole will be of the order of  $1000 \text{ km s}^{-1}$ . The UVOT light curves shown in Figure 4, in particular the light curves during the intensive daily monitoring campaign in September 2011, show that WPVS 007 can vary significantly within a few days. For a high  $L/L_{\text{Edd}}$  AGN such as WPVS 007 we can reasonably assume a standard  $\alpha$  accretion disk. The temperature stratification of an  $\alpha$  disk is described in Frank et al. (2002) and in a more appropriate form for an AGN in Peterson (1997), eq. 3.20.

The central wavelength of the W2 filter in the UVOT is at 1923Å Breeveld et al. (2010) which is equivalent to a temperature of 75000K. If we assume that WPVS 007 accretes at  $L/L_{\text{Edd}}=1$  and that the mass of the central black hole is  $4 \times 10^6 M_{\odot}$  (Leighly et al. 2009), then the UV emission in the W2 filter is emitted at  $r_{\text{UV}} = 50 R_{\text{S}}$  or  $5.8 \times 10^{11} \text{m}$ . Therefore, a dusty cloud needs

roughly two weeks to cover the UV emitting region. This is consistent within the uncertainties with the variability time scale we see from the UVOT light curves (Figure 4), which suggest a time scale of about a week.

### 4.3. NIR spectroscopy

#### 4.3.1. Emission lines

We have reported for the first time on NIR spectroscopy of WPVS 007. The NIR spectra display a variety of strong NIR emission lines as shown in Figure 8 and listed in Table 7. We compared our NIR spectra of WPVS 007 with NIR spectra of the AGN sample of Landt et al. (2008), and, in particular with the galaxies Mkn 335, Mkn 110, and PG 0844+349. This comparison shows that the NIR spectra of WPVS 007 are quite normal for a NLS1 galaxy. Although the Fe emission in WPVS 007 appears to be stronger than in Mkn 335 and PG 0844+349, it is not as strong as seen in Mkn 110 (see spectra shown in Landt et al. 2011).

#### 4.3.2. Absorption lines

As discussed in Leighly et al. (2011) (also, e.g., Fig. 1 in Leighly et al. 2012), the observation of P V predicts the presence of absorption by He I\* $\lambda$ 10833. Although this object is known to have particularly variable BALs, BAL variability is typically modest (e.g., Capellupo et al. 2012), so the IR and FUSE observations (September 2004 and November 2003, respectively) can be treated as roughly contemporaneous. In addition, the IR observation was performed after the FUSE observation. Therefore, it is probably reasonable to suppose that the outflow was still present for the IR observation, with roughly the same opacity profile. However, we see no evidence of the predicted He I absorption line in the IR spectrum.

We used the optical depth profile derived from the FUSE P V line (Leighly et al. 2009, Fig 4) to obtain an upper limit on the He I\* apparent column density, using IRAF `Specfit`. The spectrum in the region of the He I\* $\lambda$ 10833 emission line was modeled using a power law continuum and several Lorentzian line profiles. Specifically, in the vicinity of the putative absorption, our model included the following emission lines: Fe II $\lambda$ 9956, 9998, H I $\lambda$ 10052, Fe II $\lambda$ 10491, 10502, He I\* $\lambda$ 10833, H I $\lambda$ 10941, Fe II $\lambda$ 11126, and O I $\lambda$ 11290. We also

included a tiny line located at  $1.0713\ \mu\text{m}$ . Before including absorption, the width of this line was  $1150 \pm 430\text{km s}^{-1}$ , comparable to the other lines, and the equivalent width was  $\sim 3.5\ \text{\AA}$ . This line remains unidentified; it is quite near an unidentified line in Ark 564 near  $1.0740\ \text{\AA}$  (Landt et al. 2008), but it is sufficiently far away to be a different line. The IR spectra of most of the other nearby Seyfert 1 galaxies published by Landt et al. 2008 generally show no emission lines between Fe II  $\lambda\lambda 10491, 10502$  and ionHe I  $\lambda 10833$ . We included this unidentified line in our model, fixing the width and centroid, but leaving the normalization free.

Adding the absorption trough to the model, we estimated the upper limit in the He I\* column density in two ways. First, we increased the normalization of the absorption line until the  $\chi^2$  increases by 6.63 after refitting, appropriate for 99% confidence for one parameter of interest. This yielded a log He I\* column density of 12.7 for both the case when the continuum only is absorbed, and when both the emission lines and continuum are absorbed.

We also evaluated the upper limit more conservatively by increasing the depth of the absorption until the difference between the refit model and the data was comparable to the error bars on the spectrum. This criterion can only be sensibly satisfied between the He I\* emission line and the unidentified emission line, constraining our examination to the region of the absorption between  $-2760$  to  $-1480\text{ km s}^{-1}$ . As shown in Fig. 4 of Leighly et al. 2009, the optical depth is highest in this velocity range of the outflow. This procedure yielded a conservative upper limit on the log He I\* column density of 12.9, with  $\Delta\chi^2$  of 22.8 and 19.5 for absorbed continuum, and absorbed continuum plus lines, respectively. Both of these estimates are much lower than the log P V column of  $\sim 15.4$  obtained by Leighly et al. (2009). The implications of this dramatic difference will be discussed by Cooper et al. (in prep.).

In the future, additional NIR spectra of WPVS 007 will allow us to see whether any NIR features (emission or absorption lines) varied.

#### 4.4. Optical spectroscopic monitoring

Although WPVS 007 has exhibited extreme variability in X-rays as well as in the UV/optical continuum, we have shown that its optical emission lines did not exhibit any significant changes over the last two decades. This result implies, that the photoionizing continuum seen by the emission-line gas has not changed significantly over at least the last 20 years. We can therefore assume that the intrinsic spectral energy distribution of WPVS 007 has not changed much. This finding confirms the absorption scenario that we infer from our UV and X-ray observations of WPVS 007, and so most of the absorption just occurs along our line-of-sight.

#### 5. Conclusions

We presented the results from our long-term monitoring campaign of WPVS 007 between October 2005 and July 2013. This has been the longest continuous *Swift* monitoring campaign of any AGN. Our main findings are as follows:

- While remaining X-ray faint most of the time, WPVS 007 shows some remarkable fluctuations in X-ray flux during the *Swift* monitoring campaign between October 2005 and April 2013. During this period it has shown variability by factors of at least 30. In particular, it temporarily almost reached its initial ROSAT high state during one epoch in September 2009.
- The X-ray weakness seen in WPVS 007 can be explained by X-ray absorption, due to partial covering with an absorber of varying column density. During the times when the AGN is not detectable in individual observations by the *Swift* XRT, this absorption is of the order of  $4 \times 10^{23}\text{ cm}^{-2}$ . The lower absorption column densities measured during the individual X-ray detections suggest that the strong X-ray variability is primarily caused by an absorber, most-likely an outflow in the line of sight which is consistent with the BALs found in the UV spectra of WPVS 007. Clumpiness in this flow might be the reason for the large-amplitude X-ray variability seen with *Swift*.

- Applying an ionized partial covering absorber model to the X-ray data merged from all non-detections, implies that the column density and ionization parameter of the X-ray absorber is comparable with the absorber found from the UV FUSE spectra, suggesting a common origin.
- WPVS 007 is one of the most variable AGN in the UV. This is especially unusual for a NLS1. The highest amplitude of UV variability amounts to 0.66 mag within two months.
- The UV spectral variability might be caused by extinction by dusty clouds or a dusty wind. The scenario is consistent with clouds beyond the dust sublimation radius in WPVS 007 which is of the order of 20 ld (0.05 pc).
- We presented NIR spectra for the first time of WPVS 007. The rich emission-line spectra show strong Fe emission lines, neutral and singly ionized. The NIR data also show MgII, O I, OIII, and He II emission lines. Emission-line ratios are not unusual for this class of AGN. Analyzing the NIR spectra showed that the absorption column densities derived from these data are significantly lower than what has been found from the UV and X-ray data.
- New optical spectra obtained in 2011 and 2012 show that the strengths of the optical emission lines have not changed in comparison with optical data taken in the mid 1990s, implying that the underlying photoionizing continuum seen by the emission-line clouds has not changed over the last two decades.
- WPVS 007 represents an important link between BAL QSOs and NLS1s. In particular, it is a low-luminosity, low-redshift AGN that exhibits BALs that are typically present only in high-luminosity quasars at higher redshifts. Timescales in WPVS 007 are therefore shorter, making this nearby AGN an important laboratory for understanding outflows in AGN, and in BAL QSOs in particular.

We would like to thank Neil Gehrels for approving our ToO requests and the *Swift* team for performing the ToO observations of WPVS 007 and scheduling the AGN on a regular basis. Secondly, we wish to thank Kim Page for carefully reading the manuscript and for useful comments and suggestions. We would also like to thank the anonymous referee for useful comments and suggestions. Many thanks to Chris Done for her help with any questions we had regarding her *optxagnf* SED model. We want to especially thank Hermine Landt for providing the NIR spectra of her AGN sample (Landt et al. 2008, 2011) and Michael Crenshaw for making his 2007 CTIO optical spectrum (Dunn et al. 2008) available to us. This research was supported by the DFG cluster of excellence “Origin and Structure of the Universe” ([www.universe-cluster.de](http://www.universe-cluster.de)). SK would like to thank the Aspen Center for Physics for their hospitality. The Aspen Center for Physics is supported by NSF grant 1066293. This research has made use of the NASA/IPAC Extragalactic Database (NED) which is operated by the Jet Propulsion Laboratory, Caltech, under contract with the National Aeronautics and Space Administration. This publication makes use of data products from the Wide-field Infrared Survey Explorer, which is a joint project of the University of California, Los Angeles, and the Jet Propulsion Laboratory/California Institute of Technology, funded by the National Aeronautics and Space Administration. This publication makes use of data products from the Two Micron All Sky Survey, which is a joint project of the University of Massachusetts and the Infrared Processing and Analysis Center/California Institute of Technology, funded by the National Aeronautics and Space Administration and the National Science Foundation. Based on observations obtained at the Southern Astrophysical Research (SOAR) telescope, which is a joint project of the Ministério da Ciência, Tecnologia, e Inovação (MCTI) da República Federativa do Brasil, the U.S. National Optical Astronomy Observatory (NOAO), the University of North Carolina at Chapel Hill (UNC), and Michigan State University (MSU). This research has made use of the XRT Data Analysis Software (XRTDAS) developed under the responsibility of the ASI Science Data Center (ASDC), Italy. *Swift* at PSU is



supported by NASA contract NAS5-00136. This research was also supported by NASA contracts NNX07AH67G, NNX10AK85G, NNX10AF49G, and NNX11AF82G. (D.G.).

## REFERENCES

- Arnaud, K. A., 1996, ASP Conf. Ser. 101: Astronomical Data Analysis Software and Systems V, 101, 17
- Bachev, R., Grupe, D., Boeva, S., Ovcharov, E., Valcheva, A., Semkov, E., Georgiev, Ts., & Gallo, L.C., 2009, MNRAS, 399, 750
- Bans, A., & Koenigl, A., 2012, ApJ, 758, 100
- Becker, R.H., et al., 2000, ApJ, 538, 72
- Bian, W.-H., Huang, K., Hu, C., Yuan, Q.-R., Huang, K.-L., & Wang, J.-M., 2010, ApJ, 718, 460
- Boroson, T.A., & Green, R.F., 1992, ApJS, 80, 109
- Boroson, T.A., 2002, ApJ, 565, 78
- Boroson, T.A., 2011, ApJ, 735, L14
- Brandt, W.N., Laor, A., & Wills, B.J., 2000, ApJ, 528, 637
- Brandt, W.N., & Gallagher, S.C., 2000, New Astronomy Review 44, 461
- Breeveld, A.A., et al., 2010, MNRAS, 406, 1687
- Burrows, D., et al., 2005, Space Science Reviews, 120, 165
- Capellupo, D.M., et al., 2011, MNRAS, 413, 908
- Cardelli, J.A., Clayton, G.C., Mathis, J.S., 1989, ApJ, 345, 245
- Cash, W., 1979, ApJ, 228, 939
- Chiang, C.-Y., Reis, R.C., Fabian, A.C., Grupe, D., & Tsuruta, S., 2012, MNRAS, 425, 1299
- Clemens J. C., Crain J. A., Anderson R., 2004, in Moorwood A. F. M., Iye M., eds, SPIE Conf. Ser. Vol. 5492. Society of Photo-Optical Instrumentation Engineers Conf. Ser. The Goodman Spectrograph. SPIE, Bellingham, p. 331
- Crenshaw, D., Kraemer, S., & Gabel, J., 2004, ASPC, 311, 235
- Cooper, E.M., Leighly, K.M., Hamann, F., & Grupe, D., 2013, Proc. "Nuclei of Seyfert Galaxies and QSOs - Central engine and conditions of star formation",
- Dai, X., Shankar, F., & Sivakoff, G.R., 2008, ApJ, 672, 108
- Dauser, T., Svoboda, J., Schartel, N., Wilms, J., Dovciak, M., Ehle, M., Karas, V., Santos-Lleó, M., & Marshall, H.L., 2012, MNRAS, 422, 1914
- Dietrich, M., et al., 2009, ApJ, 696, 1998
- DiPompeo, M.A., Brotherton, M.S., De Breuck, C., & Laurent-Muehleisen, S., 2011, ApJ, 743, 71
- Done, C., Davis, S.W., Jin, C., Blaes, O., & Ward, M., 2012, MNRAS, 420, 1848
- Dopita, M., Hart, J., McGregor, P., et al. 2007, Ap&SS, 310, 255
- Dopita, M., Rhee, J., Farage, C., et al. 2010, Ap&SS, 327, 245
- Dunn, J.P., Crenshaw, D.M., S.B., Kraemer, & Trippe, M.L., 2008, AJ, 136, 1201
- Elvis, M., 2000, ApJ, 545, 63
- Fabian, A.C., et al., 2012, MNRAS, 419, 116
- Frank, J., King, A., & Raine, D., 2002, "Accretion Power in Astrophysics", Cambridge University Press, 3rd Edition
- Filiz Ak., N., et al., 2012, ApJ, 757, 114
- Gallo, L.C., Boller, T., Fabian, A.C., & Grupe, D., 2004, MNRAS, 352, 744
- Gallo, L. C.; Grupe, D.; Schartel, N.; Komossa, S.; Miniutti, G.; Fabian, A. C.; Santos-Lleo, M., 2011, MNRAS, 412, 161
- Gallo, L.C., et al. 2013, MNRAS, 438, 1191
- Ganguly, R., Brotherton, M.S., Cales, S., Scoggins, B., Shang, Z., & Vestergaard, M., 2007, ApJ, 665, 990

- Garcia-Rissmann, A., Rodriguez-Ardilla, A., Sigut, T.A.A., & Pradhan, A.K., 2012, *ApJ*, 751, 7
- Gehrels, N., et al., 2004, *ApJ*, 611, 1005
- Giannuzzo, M.E., & Stirpe, G.M., 1996, *A&A*, 314, 419
- Gliozzi, M., Papadakis, I.E., Grupe, D., Brinkmann, W.P., Raeth, C., & Kedziora-Chudcer, L., 2010, *ApJ*, 717, 1243
- Gliozzi, M., Papadakis, I.E., Grupe, D., Brinkmann, W.P., & Raeth, C., , 2012, *ApJ*, submitted
- Goodrich, R.W., 2000, *New Astronomy reviews*, Vol 44, 519
- Grupe, D., 2004, *AJ*, 127, 1799
- Grupe, D., Beuermann, K., Mannheim, K., Thomas, H.-C., de Martino, D., & Fink, H.H., 1995, *A&A*, 300, L21
- Grupe, D., Beuermann, K., Thomas, H.-C., Mannheim, K., & Fink, H.H., 1998, *A&A* 330, 25
- Grupe, D., Beuermann, K., Mannheim, K., & Thomas, H.-C., 1999, *A&A*, 350, 805
- Grupe, D., Leighly, K.M., Thomas, H.-C., & Laurent-Muehleisen, S.A., 2000, *A&A*, 356, 11
- Grupe, D., Thomas, H.-C., & Beuermann, K., 2001, *A&A*, 367, 470
- Grupe, D., & H.-C. Thomas, 2002, *A&A*, 386, 854
- Grupe, D., Mathur, S., & Elvis, M., 2003, *AJ*, 126, 1159
- Grupe, D., & Mathur, S., 2004, *ApJ*, 606, L41
- Grupe, D., Schady, P., Leighly, K.M., Komossa, S., O'Brien, P.T., & Nousek, J.A., 2007a, *AJ*, 133, 1988
- Grupe, D., Komossa, S., & Gallo, L.C., 2007b, *ApJ*, 668, L111
- Grupe, D., Komossa, S., Gallo, L.C., Fabian, A.C., Larsson, J., Pradhan, A.K., Xu, D., & Miniutti, G., 2008, *ApJ*, 681, 982
- Grupe, D., Leighly, K.M., & Komossa, S., 2008, *AJ*, 136, 2343
- Grupe, D., Komossa, S., Leighly, K.M., & Page, K.L., 2010, *ApJS*, 187,64
- Grupe, D., Komossa, S., Gallo, L.C., Longinotti, A.L., Fabian, A.C., Pradhan, A.K., Gruberbauer, M., & Xu, D., 2012, *ApJS*, 199, 28
- Hamann, F., Kaplan, K.F., Rodriguez Hildago, P., Prochaska, J.X., & Herbert-Fort, S., 2008, *MNRAS*, 391, L39
- Hill, J.E., et al., 2004, *SPIE*, 5165, 217
- Inoue, H., Miyakawa, T., Ebisawa, K., 2011, *PASJ*, 63, 669
- Jones, D.H., et al., 2004, *MNRAS*, 355, 747
- Jones, D.H., et al., 2009, *MNRAS*, 399, 683
- Just, D., Brandt, W.N., Shemmer, O., Steffen, A.T., Schneider, D.P., Chartas, G, & Garmire, G.P., 2007, *ApJ*,665, 1004
- Kaspi, S., Smith, P. S., Netzer, H., Maoz, D., Januzzi, B. T., & Giveon, U., 2000, *ApJ*, 533, 631
- Kishimoto, M.; Hoenic, S. F.; Antonucci, R.; Millour, F.; Tristram, K. R. W.; Weigelt, G., 2011, *A&A*, 536, 78
- Klimek, E.S., Gaskell, C.M., & Hedrick, C.H., 2004, *ApJ*, 609, 69
- Kollatschny, W., Fricke, K.J., Schleicher, H., & Yorke, H.W., 1981, *A&A*, 102, L23
- Kollatschny, W., & Fricke, K.J., 1985, *A&A*, 146, L11
- Kollatschny, W., Bischoff, K., & Dietrich, M., 2000, *A&A*, 361, 901
- Komossa, S., 2008, *RMxAC*, 32, 86
- Komossa, S., et al., 2008a, *ApJ*, 678, L13
- Komossa, S., et al., 2008b, *ApJ*, 680, 926
- Kraft, R.P., Burrows, D.N., & Nousek, J.A., 1991, *ApJ*, 374, 344
- Kurasawa, R., & Proga, D., 2009a, *ApJ*, 693, 1929

- Kurasawa, R., & Proga, D., 2009b, MNRAS, 397, 1791
- Landt, H., Bentz, M.C., Ward, M.J., Elvis, M., Peterson, B.M., Korista, K.T., & Karovska, M., 2008, ApJS, 174, 282
- Landt, H., Elvis, M., Ward, M.J., Bentz, M.C., Korista, K.T., & Karovska, M., 2011, MNRAS, 414, 218
- Laor, A., & Brandt, W.N., 2002, ApJ, 569, 641
- Leighly, K.M., Halpern, J.P., Jenkins, E.B., Grupe, D., Choi, J., & Prescott, K.B., 2007, ApJ, 663, 103
- Leighly, K.M., Halpern, J.P., Jenkins, E.B., & Casebeer, D., 2007, ApJS, 173, 1
- Leighly, K.M., Hamann, F., Casebeer, D.A., & Grupe, D., 2009, ApJ, 701, 176
- Leighly, K. M., Dietrich, M., & Barber, S., 2011, ApJ, 728, 94
- Leighly, K. M., Lucy, A. B., Dietrich, M., Terndrup, D., & Gallagher, S. C., 2012, in Proc. "AGN Winds in Charleston", Eds. G. Chartas, F. Hamann, & K. M. Leighly (San Francisco: Astronomical Society of the Pacific), p. 72
- Lobban, A. P., Reeves, J. N., Miller, L., Turner, T. J., Braitto, V., Kraemer, S. B., & Crenshaw, D. M., 2011, MNRAS, 414, 1965
- Lohfink, A.M., Reynolds, C.S., Miller, J.M., Brenneman, L.W., Mushotzky, R.F., Nowak, M.A., & Fabian, A.C., 2012, ApJ, 758, 67
- Longinotti, A.L., et al., 2013, ApJ, 766, 104
- Marziani, P., et al., 2009, A&A, 495, 83
- Mathur, S., 2000, MNRAS, 314, L17
- Miller, L., Turner, J.T., Reeves, J.N., & Braitto, V., 2010, MNRAS, 408, 1928
- Miniutti, G., Brandt, W.N., Schneider, D.P., Fabian, A.C., Gallo, L.C., & Boller, T., 2012, MNRAS, accepted, arXiv:1207:0694v1
- Osterbrock, D.E., & Pogge, R.W., 1985, ApJ, 297, 166
- Peterson, B.M., 1997, "Active Galactic Nuclei", Cambridge University Press
- Pfeffermann E., Briel U.G., Hippmann H., et al., 1986, SPIE 733, 519
- Park, T., Kashyap, V.L., Siemiginowska, A., van Dyk, D.A., Zezas, A., Heinke, C., & Wargelin, B.J., 2006, ApJ, 652, 610
- Poole, T.S., et al., 2008, MNRAS, 383, 627
- Proga, D., & Kallman, T.R., 2004, ApJ, 616, 688
- Ralchenko, Y., Kramida, A.E., Reader, J., and NIST ASD Team, 2011, NIST Atomic Spectra Database (ver. 4.1.0), [Online]. Available: <http://physics.nist.gov/asd> National Institute of Standards and Technology, Gaithersburg, MD.
- Reeves, J., et al., 2008, MNRAS, 385, L108
- Reynolds, C.S., & Nowak, M.A., 2003, Physics Reports, 377, 6, 389
- Rodriguez-Ardila, A., Prieto, M.A., Portilla, J.G., & Tejeiro, J.M., 2011, ApJ, 743, 100
- Roming, P.W.A., et al., 2005, Space Science Reviews, 120, 95
- Roming, P.W.A., et al., 2009, ApJ, 690, 163
- Saez, C., Brandt, W.N., Gallagher, S.C., Bauer, F.E., & Garmire, G.P., 2012, ApJ, 759, 42
- Schartel, N., Rodríguez-Pascual, P. M., Santos-Lleó, M., Jiménez-Bailón, E., Ballo, L.; Piconcelli, E. 2010, A&A, 512, 75
- Schartel, N., Grupe, D, Santos-Lleó, M., Komossa, S., Gallo, L.C., Fabian, A.C., & Miniutti, G., 2013, A&A, letter, submitted
- Schlegel, D. J., Finkbeiner, D. P., & Davis, M. 1998, ApJ, 500, 525
- Schwöpe, A.D., et al., 2000, Astronomische Nachrichten, 321, 1
- Shapovalova, A.I., et al., 2012, ApJS, 202, 10
- Strateva, I.V., Brandt, W.N., Schneider, D.P., Vanden Berk, D.G., & Vignali, C., 2005, AJ, 130, 387

- Sulentic, J.W., Zwitter, T., Marziani, P., & Dultzin-Hacyan, D., 2000, *ApJ*, 536, L5
- Tananbaum, H., et al., 1979, *ApJ*, 234, L9
- Vaughan, S., Edelson, R., & Warwick, R.S., 2004, *MNRAS*, 349, L1
- Vestergaard, M., & Peterson, B.M., 2005, *ApJ*, 625, 688
- Voges, W., Aschenbach, B., Boller, T., et al., 1999, *A&A*, 349, 389
- Wamsteker, W., Prieto A., Vitores, A., Schuster, H.E., Danks, A.C., Gonzalez R., & Rodriguez, G., 1985, *A&AS*, 62, 255
- Weymann, R.J., Morris, L., Foltz, C.B., & Hewitt, P.C., 1991, *ApJ*, 373, 23
- Williams, R.J., Pogge, R.W., & Mathur, S., 2002, *AJ*, 124, 3042
- Williams, R.J., Mathur, S., & Pogge, R.W., 2004, *ApJ*, 610, 737
- Wright, E.L., 2006, *PASP*, 118, 1711
- Wu, J., et al., 2011, *ApJ*, 736, 28
- Xu, D., et al., 2012, *AJ*, 143, 83



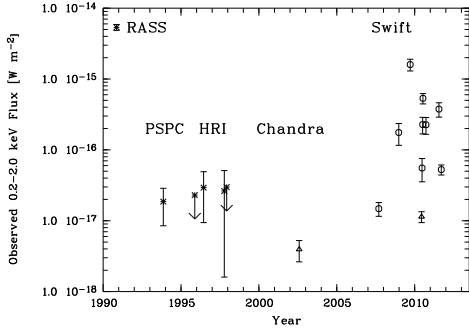


Fig. 2.— Long-term 0.2-2.0 keV X-ray light curve of WPVS 007 starting with the ROSAT All-Sky Survey observation in November 1990. ROSAT observations are marked as stars, Chandra data as triangles, *Swift* detections (Table 4) as open circles. Note that the detection limit of the *Swift* XRT for a 5ks observation is about  $4 \times 10^{-17}$   $\text{W m}^{-2}$ .

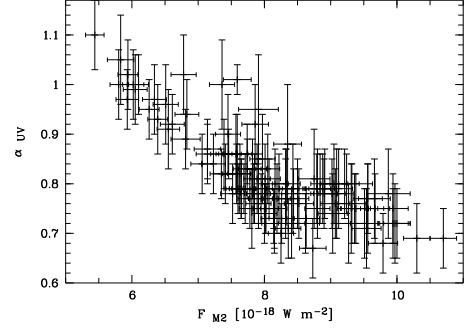


Fig. 5.— Flux in the UVOT M2 filter vs optical/UV spectral slope  $\alpha_{UV}$

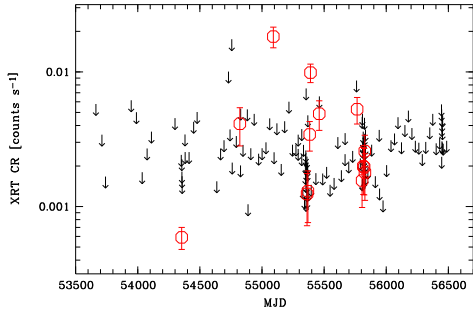


Fig. 3.— *Swift* XRT  $3\sigma$  upper limits (downward arrows) and detections (open circles) of WPVS 007 as listed in Tables 3 and 4, and Table 1 in Grupe et al. (2007a).

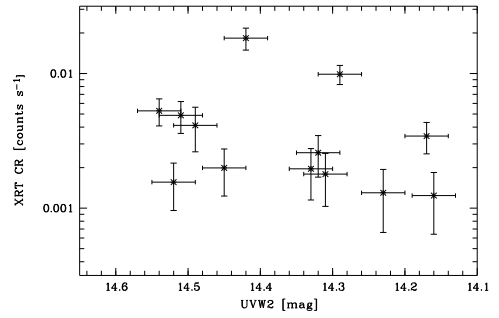


Fig. 6.— UVOT W2 magnitude vs. XRT count rate during detections (See Table 4).

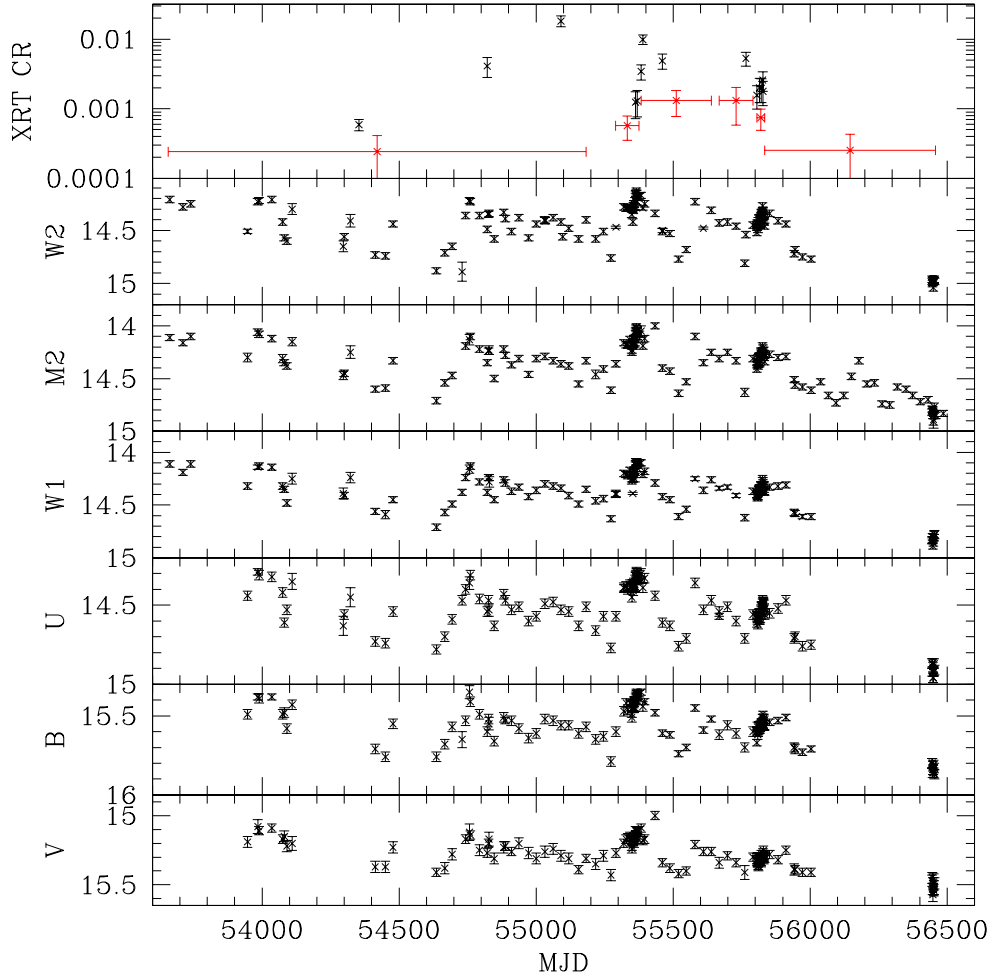


Fig. 1.— *Swift* XRT and UVOT light curves of WPVS 007 starting in 2005 October until 2013 July. The X-ray detections of WPVS 007 are listed in Table 4 and all reddening corrected UVOT magnitudes are listed in Table 2. The red data points mark the long-term detections of WPVS 007 when it was undetected in a single observation. Data were added until the source was detected at a  $3\sigma$  level.

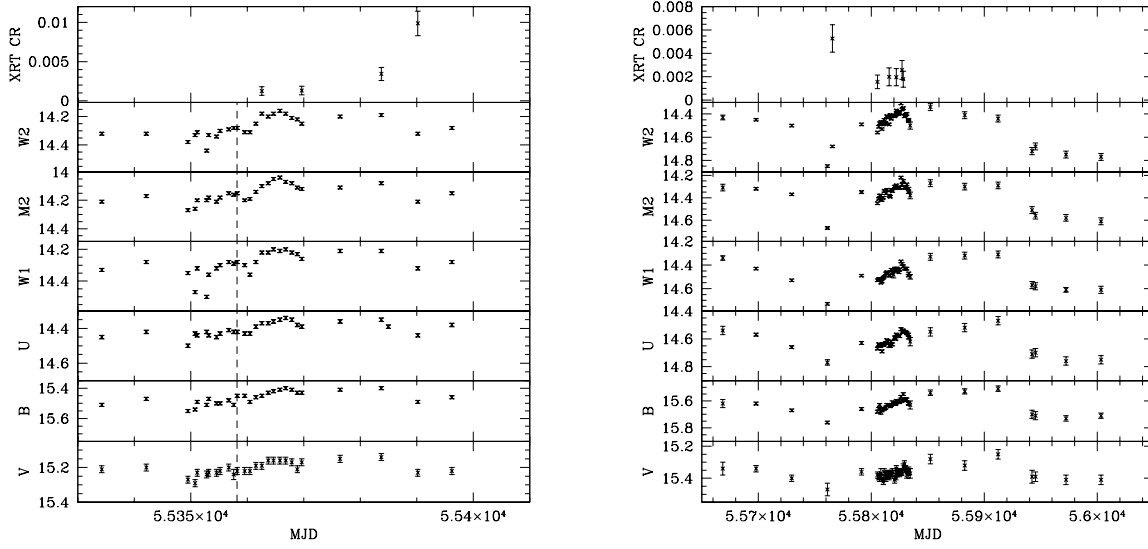


Fig. 4.— XRT and UVOT light curves during and around the intense monitoring campaigns in June 2010 and September 2011 (2010-June-02 = MJD 55349, and 2011-September-01 = MJD 55805). Note that only detections in the XRT are shown. During all other observations only  $3\sigma$  upper limits can be given as shown in Figure 3.

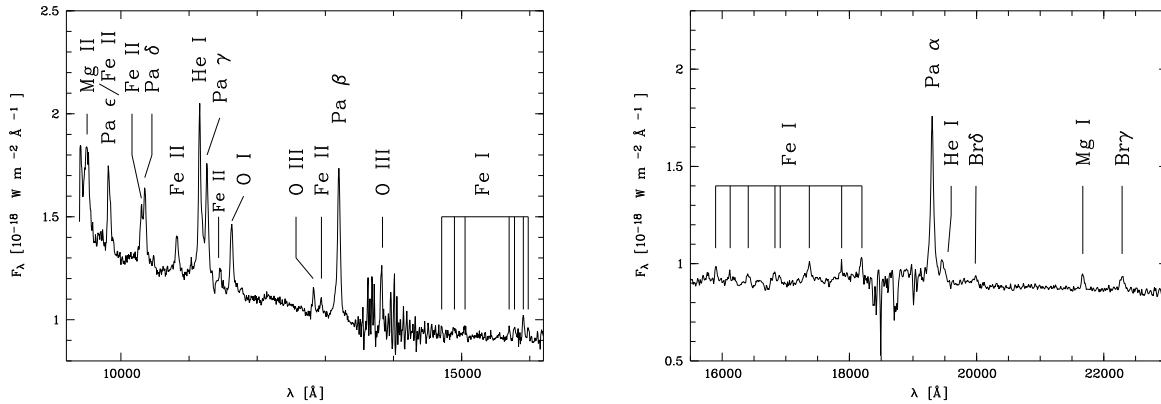


Fig. 8.— Near Infrared spectrum of WPVS 007 in the J plus H and H plus K wavelength bands observed on 2004 September 12 with the 3.5m ESO NTT. Note that the noise around  $1.4\mu\text{m}$  and short of  $\text{Pa}\alpha$  is due to correction for atmospheric absorption.

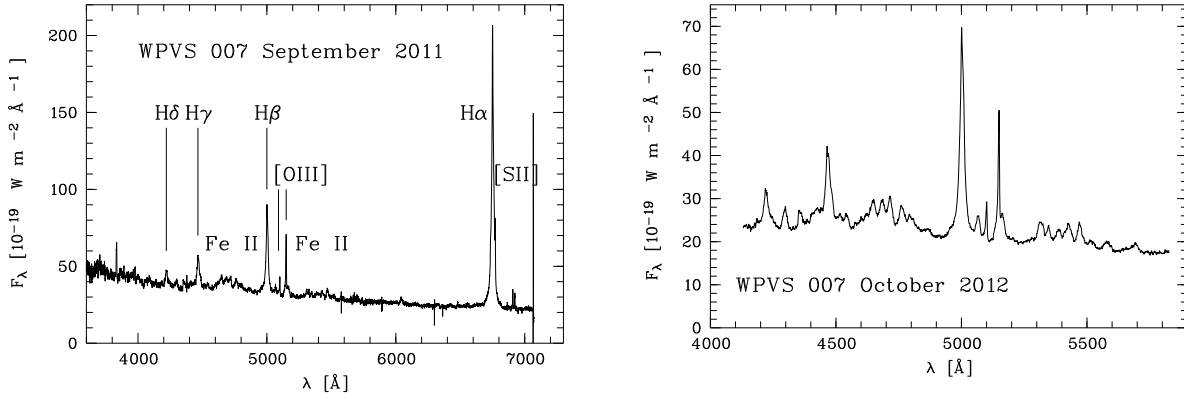


Fig. 10.— Optical spectrum of WPVS 007 obtained in September 2011 at the ANU 2.3m telescope at Siding Spring Observatory using the 3" extraction radius, and the 4.1m SOAR telescope in October 2012 (left and right panels, respectively).

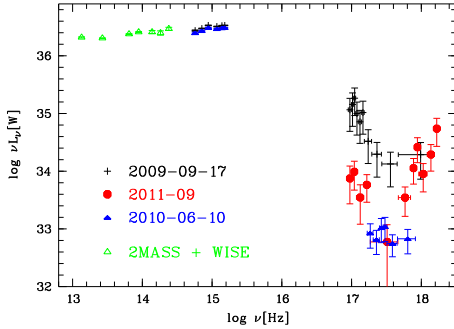


Fig. 7.— Spectral Energy Distributions of WPVS 007 during the *Swift* observations from 2009 September 17 and 2011 September, and the *Chandra* observation on 2010 June 10. Note that the X-ray data have been rebinned for display purposes, and that the WISE and 2MASS data in the Mid and Near Infrared are non-contemporaneous. Note that only the UVOT data from 2009 September 17 and 2010 June 10 are shown.

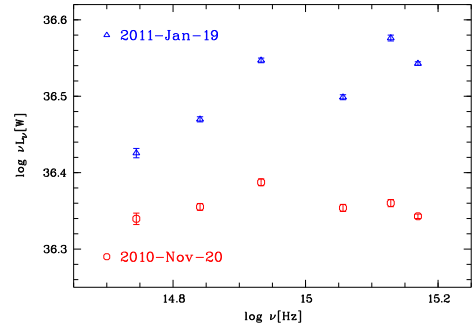


Fig. 9.— *Swift* UVOT Observations of WPVS 007 during the low and high state on 2010 November 20 and 2011 January 19, respectively. UVOT filter with increasing frequency are: V, B, U, W1, M2, and W2.



TABLE 1  
*Swift* OBSERVATION LOG OF WPVS 007 AFTER JANUARY 2008<sup>1</sup>

ObsID	Segment	T-start <sup>2</sup>	T-stop <sup>2</sup>	MJD	T <sub>XRT</sub> <sup>3</sup>	T <sub>V</sub> <sup>3</sup>	T <sub>B</sub> <sup>3</sup>	T <sub>U</sub> <sup>3</sup>	T <sub>UVW1</sub> <sup>3</sup>	T <sub>UVM2</sub> <sup>3</sup>	T <sub>UVW2</sub> <sup>3</sup>
30334	030	2008-01-12 17:56	2008-01-12 22:55	54477.85	1528	144	156	156	310	260	623
	031	2008-06-19 00:03	2008-06-19 06:42	54636.14	3753	334	334	334	668	874	1337
	032	2008-07-19 15:28	2008-07-19 17:28	54666.69	2140	176	176	176	352	443	704
	033	2008-08-16 02:28	2008-08-16 05:57	54694.18	1854	153	153	153	306	383	614
	034	2008-09-21 09:11	2008-09-21 12:27	54730.45	546	...	36	114	346	...	21
	035	2008-10-03 13:41	2008-10-03 18:41	54742.67	2046	214	214	214	428	350	653
	036	2008-10-17 16:26	2008-10-17 16:34	54756.69	452	41	41	41	83	74	165
	037	2008-10-21 05:22	2008-10-21 07:21	54760.27	2721	230	230	230	460	587	921
	038	2008-11-23 00:27	2008-11-23 03:52	54793.10	2125	153	197	197	395	308	790
	039	2008-12-21 14:25	2008-12-21 16:21	54821.64	2330	215	215	215	430	334	862
	040	2008-12-27 00:25	2008-12-27 03:52	54827.09	2863	241	242	242	484	601	968
	041	2008-12-28 00:33	2008-12-28 07:00	54828.16	1081	71	71	71	389	164	283
	042	2008-12-29 02:16	2008-12-29 07:05	54829.19	47	...	...	...	47	...	...
	043	2009-01-16 00:50	2009-01-16 02:43	54847.08	2011	166	166	166	332	459	665
	044	2009-02-19 21:56	2009-02-19 23:49	54881.95	2131	181	181	178	359	448	724
	045	2009-02-25 07:57	2009-02-25 22:39	54887.64	7042	583	583	622	1299	1341	2337
	046	2009-03-19 17:57	2009-03-19 23:09	54909.85	2808	237	237	237	474	586	948
	047	2009-04-16 00:03	2009-04-16 01:45	54937.03	1587	141	141	141	283	395	567
	048	2009-05-21 19:33	2009-05-21 22:52	54972.88	2343	197	197	197	395	483	790
90108	001	2009-06-18 20:36	2009-06-18 22:31	55000.90	2144	176	176	176	352	502	704
	002	2009-07-19 18:31	2009-07-19 20:24	55031.80	2697	171	171	171	342	330	685
	003	2009-07-21 01:03	2009-07-21 01:08	55033.04	281	...	...	...	...	...	277
	004	2009-08-19 00:38	2009-08-19 02:36	55062.07	2084	176	176	176	352	436	704
	005	2009-09-17 01:31	2009-09-19 03:22	55091.09	1818	151	151	151	303	410	606
	006	2009-09-23 00:39	2009-09-23 05:45	55097.15	6266	...	...	...	...	...	6202
	007	2009-10-15 19:05	2009-10-15 20:50	55119.83	1875	156	156	156	313	396	626
	008	2009-11-19 17:11	2009-11-19 23:48	55154.85	2799	230	230	230	461	586	924
	009	2009-12-17 06:46	2009-12-17 10:11	55182.35	2621	217	217	217	434	567	869
	010	2010-01-21 00:34	2010-01-21 02:23	55217.06	1882	176	176	176	352	228	704
	011	2010-02-18 11:19	2010-02-18 13:08	55245.51	2007	171	171	171	342	403	685
	012	2010-03-18 08:59	2010-03-18 11:05	55273.42	2002	166	166	166	332	456	665
90331	001	2010-04-05 00:49	2010-04-05 04:29	55291.11	2848	235	235	235	470	663	941
	002	2010-04-05 02:28	2010-04-05 06:10	55291.18	2234	...	...	...	2215	...	...
	003	2010-05-04 00:29	2010-05-04 03:59	55320.09	3090	251	251	251	503	722	1007
	004	2010-05-04 05:18	2010-05-04 07:12	55320.26	2040	...	...	2019	...	...	...
	005	2010-05-12 17:12	2010-05-12 23:45	55328.85	4163	339	338	339	678	935	1357
	006	2010-05-18 03:22	2010-05-18 08:42	55334.20	4417	302	430	430	861	666	1602
	007	2010-05-26 00:47	2010-05-26 05:58	55342.14	4927	430	430	430	861	1239	1723
	008	2010-06-02 09:24	2010-06-02 14:32	55349.50	4315	361	361	361	723	903	1448
	009	2010-06-03 14:25	2010-06-03 21:18	55349.75	3239	319	319	319	389	946	1074
	010	2010-06-04 01:48	2010-06-04 06:47	55351.08	5110	425	425	425	851	1222	1704
	011	2010-06-05 16:13	2010-06-05 22:55	55352.81	3603	337	337	337	738	932	1350
	012	2010-06-06 00:15	2010-06-06 06:52	55353.15	4994	407	407	407	816	1159	1633
	013	2010-06-07 11:36	2010-06-07 18:16	55354.60	5155	358	358	358	717	1755	1435
	014	2010-06-08 02:06	2010-06-08 07:12	55355.20	3583	301	301	301	602	788	1204
	015	2010-06-09 15:04	2010-06-09 20:14	55356.73	4906	415	416	415	832	1162	1664
	016	2010-06-10 12:15	2010-06-10 17:14	55357.62	3594	185	415	416	832	442	1201
	017	2010-06-11 04:02	2010-06-11 07:42	55357.24	5029	414	414	414	828	1182	1657
	018	2010-06-12 10:33	2010-06-12 15:43	55359.55	4887	396	396	396	792	1172	1586
	019	2010-06-13 09:07	2010-06-13 14:08	55360.48	5333	440	440	440	881	1216	1763
	020	2010-06-14 09:22	2010-06-14 15:55	55361.52	4652	381	381	381	763	1084	1527
	021	2010-06-15 10:49	2010-06-15 17:32	55362.59	5020	407	407	407	816	1169	1633
	022	2010-06-16 10:57	2010-06-16 24:00	55363.73	4900	404	404	404	810	969	1624
	023	2010-06-17 08:08	2010-06-17 22:50	55364.65	5570	452	452	452	904	1328	1810
	024	2010-06-18 14:24	2010-06-18 22:56	55365.78	5335	437	437	437	875	1214	1750
	025	2010-06-19 15:58	2010-06-19 23:02	55366.81	5732	452	452	452	904	1489	1810
	026	2010-06-20 17:48	2010-06-21 00:32	55367.89	5118	420	420	420	842	1188	1684
	027	2010-06-21 17:51	2010-06-21 23:07	55368.85	6009	450	450	450	901	1812	1802
	028	2010-06-22 13:01	2010-06-22 18:17	55369.65	4848	396	396	396	792	1127	1586
	029	2010-06-29 02:44	2010-06-29 17:24	55376.40	4288	350	350	350	701	979	1404
	030	2010-07-06 14:18	2010-07-06 21:01	55383.74	5218	427	427	427	855	1188	1711
30334	049	2010-07-07 20:54	2010-07-08 02:04	55384.98	4678	...	...	4849	...	...	...
90331	031	2010-07-13 00:29	2010-07-13 08:28	55390.19	4111	348	348	348	698	836	1397
	032	2010-07-19 01:04	2010-07-19 09:21	55396.22	5146	423	423	424	849	1150	1699
	033	2010-08-25 17:06	2010-08-25 20:41	55433.79	4190	345	345	345	690	967	1381
	034	2010-09-21 11:39	2010-09-21 21:45	55460.69	3516	297	297	297	596	707	1192
	035	2010-09-22 14:59	2010-09-22 16:40	55461.66	1470	...	...	...	...	...	1468
	036	2010-10-19 07:35	2010-10-19 11:17	55488.39	5111	433	433	433	867	1155	1736
	037	2010-11-20 01:06	2010-11-20 07:56	55520.15	5449	447	447	447	895	1255	1790
	038	2010-12-18 05:02	2010-12-18 08:44	55548.29	5103	419	419	419	838	1225	1790
	039	2011-01-19 01:26	2011-01-19 09:51	55580.24	4571	465	465	465	930	1237	1861
	040	2011-02-18 09:04	2011-02-18 14:07	55610.48	5224	415	415	414	830	1339	1660
	041	2011-03-19 00:08	2011-03-19 02:12	55639.04	3103	264	264	264	528	769	1059
91017	001	2011-04-17 15:31	2011-04-17 19:02	55668.72	3092	251	251	251	503	730	1007
	002	2011-04-17 20:26	2011-04-17 22:15	55668.89	2026	...	...	2009	...	...	...
	003	2011-05-17 00:16	2011-05-17 05:37	55698.10	4213	338	338	338	677	729	1348
	004	2011-06-17 12:41	2011-06-17 17:49	55729.64	4844	394	394	394	591	1144	1183
	005	2011-07-19 04:08	2011-07-19 04:27	55761.18	1118	90	90	90	181	239	362
	006	2011-07-23 12:13	2011-07-23 15:50	55765.58	4750	...	...	...	...	...	4708
	007	2011-08-18 01:14	2011-08-18 16:32	55791.38	3277	274	274	274	549	763	1098
	008	2011-09-01 05:51	2011-09-01 17:45	55805.49	5377	429	429	429	659	1019	1316
	009	2011-09-02 09:18	2011-09-02 17:20	55806.56	3444	275	275	275	550	855	1101
	010	2011-09-03 07:39	2011-09-03 12:47	55807.42	4544	369	369	369	735	1140	1473
	011	2011-09-04 10:58	2011-09-04 12:49	55808.49	2280	185	185	182	179	246	358
	012	2011-09-05 01:43	2011-09-05 22:51	55809.51	4588	366	366	366	735	1084	1472
	013	2011-09-06 09:26	2011-09-06 22:55	55810.65	5036	399	400	400	802	1239	1605

TABLE 1—Continued

ObsID	Segment	T-start <sup>2</sup>	T-stop <sup>2</sup>	MJD	T <sub>XRT</sub> <sup>3</sup>	T <sub>V</sub> <sup>3</sup>	T <sub>B</sub> <sup>3</sup>	T <sub>U</sub> <sup>3</sup>	T <sub>UVW1</sub> <sup>3</sup>	T <sub>UVM2</sub> <sup>3</sup>	T <sub>UVW2</sub> <sup>3</sup>
	014	2011-09-07 00:12	2011-09-07 18:11	55811.38	4745	388	388	388	586	1034	1554
	015	2011-09-08 14:30	2011-09-08 22:43	55812.77	4999	408	408	445	893	1077	1634
	016	2011-09-09 16:09	2011-09-09 19:53	55813.75	5078	413	413	413	826	1236	1653
	017	2011-09-10 16:16	2011-09-10 19:57	55814.75	4987	406	407	407	546	1229	1626
	018	2011-09-11 16:20	2011-09-11 20:02	55815.76	5032	412	412	412	825	1236	1650
	019	2011-09-12 16:25	2011-09-12 20:06	55816.76	4304	281	412	412	930	838	839
	020	2011-09-13 16:30	2011-09-13 20:10	55817.76	5027	420	420	420	840	1163	1679
	021	2011-09-14 14:58	2011-09-14 18:40	55818.70	5186	434	433	433	578	773	1735
	022	2011-09-15 17:07	2011-09-15 18:45	55819.75	152	...	...	...	66	...	...
	023	2011-09-16 15:09	2011-09-16 18:50	55820.71	5029	407	407	407	811	1258	1623
	024	2011-09-17 16:51	2011-09-17 22:08	55821.81	4938	397	397	397	795	1234	1592
	025	2011-09-18 01:09	2011-09-18 09:12	55822.22	5201	427	427	427	732	1184	1470
	026	2011-09-19 00:57	2011-09-19 06:03	55823.15	4195	350	350	350	512	930	1024
	027	2011-09-20 04:21	2011-09-20 17:27	55824.45	4541	391	391	391	783	937	1566
	028	2011-09-21 01:09	2011-09-21 04:50	55825.12	3172	419	419	419	559	1085	1677
	029	2011-09-22 01:17	2011-09-22 12:59	55826.31	4598	379	379	379	759	1056	1518
	030	2011-09-23 01:29	2011-09-23 13:05	55827.30	4650	379	379	379	760	1105	1520
	031	2011-09-24 01:28	2011-09-24 19:36	55828.44	4860	394	394	394	787	1200	1576
	032	2011-09-25 03:11	2011-09-25 18:05	55829.45	3808	264	356	367	872	799	1061
	033	2011-09-26 01:40	2011-09-26 18:10	55830.41	4792	392	392	392	787	752	1572
	034	2011-09-27 03:21	2011-09-27 13:27	55831.43	4367	365	365	365	730	956	1460
	035	2011-09-28 19:37	2011-09-28 23:16	55832.89	4819	409	279	409	818	694	1637
	036	2011-09-29 00:17	2011-09-29 03:53	55833.08	4561	384	384	384	500	645	1000
	037	2011-09-30 02:07	2011-09-30 21:40	55834.51	4768	396	396	396	720	965	1440
	038	2011-10-18 03:12	2011-10-18 16:22	55852.41	3674	340	340	340	289	740	579
	039	2011-11-17 13:46	2011-11-17 17:27	55882.65	4967	397	397	397	795	1275	1591
	040	2011-12-17 04:23	2011-12-17 09:36	55912.29	4200	347	347	347	693	950	1387
	041	2012-01-17 09:53	2012-01-17 15:01	55943.52	2031	192	192	192	383	372	767
	042	2012-01-20 08:28	2012-01-20 13:34	55946.46	4250	348	347	348	696	980	1390
	043	2012-02-17 00:31	2012-02-17 23:21	55974.50	5209	425	421	425	849	1211	1701
	044	2012-03-17 02:43	2012-03-17 12:44	56003.31	4453	246	410	410	821	911	1493
30334	050	2012-04-21 00:05	2012-04-21 14:59	56038.31	1935	...	...	...	...	1976	...
	051	2012-05-19 16:09	2012-05-19 19:39	56066.75	2170	...	...	...	...	2151	...
	052	2012-06-16 09:45	2012-06-16 19:51	56094.62	1661	...	...	...	...	1647	...
	053	2012-07-14 16:21	2012-07-14 21:20	56122.79	1933	...	...	...	...	1905	...
	054	2012-08-11 00:23	2012-08-11 21:24	56150.44	1883	...	...	...	...	1958	...
	055	2012-09-08 06:30	2012-09-08 08:00	56178.30	1875	...	...	...	...	1865	...
	056	2012-10-06 20:46	2012-10-06 22:20	56206.89	1998	...	...	...	...	1978	...
	057	2012-11-03 06:10	2012-11-03 15:51	56234.48	1883	...	...	...	...	1866	...
	058	2012-12-01 05:57	2012-12-01 12:24	56262.38	1953	...	...	...	...	1930	...
	059	2012-12-29 13:18	2012-12-29 15:10	56290.59	2370	...	...	...	...	2345	...
	060	2013-01-26 03:26	2013-01-26 05:17	56318.18	1923	...	...	...	...	1909	...
	062	2013-02-27 06:22	2013-02-27 08:07	56350.30	1968	...	...	...	...	1954	...
	063	2013-03-23 10:44	2013-03-23 12:39	56374.49	1943	...	...	...	...	1939	...
	064	2013-04-20 00:26	2013-04-20 05:26	56402.12	2577	...	...	...	...	2604	...
	065	2013-05-18 00:06	2013-05-18 03:25	56430.08	1771	...	...	...	...	1835	...
	066	2013-06-01 17:42	2013-06-01 19:34	56444.77	1678	136	136	136	274	414	550
	067	2013-06-02 20:59	2013-06-02 23:02	56445.92	2335	192	193	192	384	544	770
	068	2013-06-03 09:48	2013-06-03 23:04	56446.69	2465	197	197	197	396	624	792
	069	2013-06-04 19:40	2013-06-04 21:32	56447.85	1913	151	151	151	304	474	609
	070	2013-06-05 08:30	2013-06-05 16:46	56448.53	1900	151	151	151	303	473	605
	071	2013-06-06 13:23	2013-06-06 16:43	56449.63	1973	160	160	160	320	454	640
	072	2013-06-07 08:39	2013-06-07 10:26	56450.40	1321	65	154	154	309	47	551
	073	2013-06-08 11:43	2013-06-08 13:38	56451.53	1943	160	160	160	320	429	641
	074	2013-06-09 19:47	2013-06-09 21:39	56452.87	1518	125	140	140	282	218	563
	075	2013-06-10 21:28	2013-06-10 23:18	56453.93	1638	139	139	139	140	330	561
	076	2013-06-15 12:04	2013-06-15 13:58	56458.54	1980	...	...	...	...	1975	...
	077	2013-07-13 03:22	2013-07-13 22:56	56486.48	1895	...	...	...	...	1884	...

<sup>1</sup>Observing times prior to January 2008 can be found in Grupe et al. (2007a) and Grupe et al. (2008b).

<sup>2</sup>Start and end times are given in UT

<sup>3</sup>Observing time given in s

TABLE 2  
*Swift* UVOT MAGNITUDES OF WPVS 007

ObsID	Segment	MJD	V	B	U	UVW1	UVM2	UVW2	$\alpha_{UV}$
30334	001	53663.15	...	...	...	14.11±0.03	14.11±0.03	14.21±0.03	...
	002	53711.57	...	...	...	14.19±0.03	14.16±0.03	14.28±0.03	...
	003	53740.16	...	...	...	14.11±0.03	14.10±0.03	14.25±0.03	...
	004	53947.23	15.19±0.04	15.49±0.03	14.44±0.03	14.32±0.03	14.30±0.04	14.51±0.02	0.95±0.11
	005	53984.42	15.08±0.05	15.38±0.02	14.29±0.02	14.14±0.02	14.06±0.03	14.23±0.03	0.78±0.09
	006	53989.28	15.11±0.03	15.39±0.03	14.31±0.03	14.13±0.03	14.08±0.03	14.22±0.03	0.77±0.08
	007	54035.64	15.09±0.03	15.38±0.02	14.32±0.03	14.14±0.03	14.12±0.03	14.21±0.03	0.80±0.07
	008	54075.14	15.17±0.03	15.49±0.03	14.42±0.03	14.32±0.03	14.31±0.04	14.42±0.03	0.92±0.08
	009	54081.03	15.15±0.04	15.48±0.03	14.61±0.03	14.35±0.03	14.35±0.03	14.57±0.03	1.01±0.03
	010	54090.30	15.22±0.04	15.58±0.03	14.53±0.03	14.48±0.03	14.38±0.03	14.60±0.03	1.00±0.09
	011	54110.04	15.20±0.05	15.43±0.03	14.35±0.05	14.25±0.05	14.15±0.04	14.30±0.05	0.78±0.09
	012	54296.40	...	...	14.63±0.06	14.39±0.05	14.47±0.04	14.65±0.05	...
	013	54299.81	...	...	14.56±0.03	14.41±0.03	14.45±0.03	14.56±0.03	...
	014	54322.59	...	...	14.45±0.06	14.24±0.05	14.25±0.06	14.41±0.06	...
	028	54413.06	15.37±0.04	15.71±0.03	14.73±0.03	14.56±0.03	14.60±0.03	14.73±0.03	1.00±0.07
	029	54449.70	15.37±0.04	15.76±0.03	14.74±0.03	14.59±0.04	14.59±0.03	14.74±0.03	0.99±0.07
	030	54477.85	15.23±0.04	15.55±0.03	14.54±0.03	14.45±0.03	14.33±0.03	14.44±0.03	0.86±0.06
	031	54636.14	15.41±0.03	15.76±0.03	14.78±0.03	14.71±0.03	14.71±0.03	14.88±0.03	1.10±0.07
	032	54666.69	15.38±0.04	15.68±0.03	14.70±0.03	14.57±0.03	14.54±0.03	14.71±0.03	0.97±0.07
	033	54694.18	15.28±0.04	15.57±0.03	14.59±0.03	14.49±0.03	14.47±0.03	14.65±0.03	1.02±0.08
	034	54730.45	...	15.65±0.05	14.47±0.03	14.38±0.03	...	14.89±0.09	1.35±0.43
	035	54742.67	15.17±0.03	15.53±0.03	14.40±0.03	14.24±0.03	14.19±0.03	14.36±0.03	0.81±0.10
	036	54756.69	15.12±0.06	15.35±0.04	14.36±0.04	14.16±0.04	14.13±0.05	14.22±0.03	0.80±0.06
	037	54760.27	15.14±0.03	15.41±0.03	14.31±0.03	14.13±0.03	14.10±0.03	14.23±0.03	0.75±0.09
	038	54793.10	15.25±0.04	15.49±0.03	14.46±0.03	14.28±0.03	14.22±0.03	14.36±0.03	0.78±0.07
	039	54821.64	15.27±0.03	15.60±0.03	14.54±0.03	14.38±0.03	14.35±0.03	14.49±0.03	0.86±0.08
	040	54827.09	15.20±0.03	15.52±0.03	14.47±0.03	14.24±0.03	14.24±0.03	14.35±0.03	0.80±0.07
	041	54828.16	15.17±0.05	15.55±0.04	14.53±0.04	14.24±0.03	14.23±0.04	14.34±0.03	0.77±0.06
	042	54829.19	...	...	...	14.28±0.05	...	...	...
	043	54847.08	15.31±0.04	15.66±0.03	14.63±0.03	14.45±0.03	14.50±0.03	14.58±0.03	0.92±0.06
	044	54881.95	15.23±0.04	15.51±0.03	14.43±0.03	14.26±0.03	14.22±0.03	14.33±0.03	0.76±0.07
	045	54887.64	15.22±0.03	15.53±0.02	14.47±0.03	14.29±0.03	14.28±0.03	14.39±0.03	0.83±0.07
	046	54909.85	15.26±0.03	15.53±0.03	14.53±0.03	14.37±0.03	14.37±0.03	14.51±0.03	0.90±0.08
	047	54937.03	15.20±0.04	15.58±0.03	14.51±0.03	14.33±0.03	14.31±0.03	14.38±0.03	0.83±0.06
	048	54972.88	15.27±0.04	15.64±0.03	14.60±0.03	14.42±0.03	14.46±0.03	14.57±0.03	0.94±0.07
90108	001	55000.90	15.31±0.04	15.61±0.03	14.57±0.03	14.36±0.03	14.31±0.03	14.44±0.03	0.78±0.06
	002	55031.80	15.26±0.04	15.52±0.03	14.49±0.03	14.30±0.03	14.29±0.03	14.40±0.03	0.81±0.07
	003	55035.04	...	...	...	...	...	14.41±0.03	...
	004	55062.07	15.24±0.04	15.53±0.03	14.48±0.03	14.32±0.03	14.33±0.03	14.38±0.03	0.83±0.06
	005	55091.09	15.29±0.04	15.56±0.03	14.53±0.03	14.34±0.03	14.36±0.03	14.42±0.03	0.82±0.06
	006	55097.15	...	...	...	...	...	14.56±0.03	...
	007	55119.83	15.31±0.04	15.56±0.03	14.54±0.03	14.41±0.03	14.38±0.03	14.48±0.03	0.86±0.07
	008	55154.85	15.39±0.03	15.61±0.03	14.63±0.03	14.49±0.03	14.55±0.03	14.58±0.03	0.91±0.08
	009	55182.35	15.31±0.03	15.57±0.03	14.51±0.03	14.35±0.03	14.33±0.03	14.40±0.03	0.79±0.07
	010	55217.06	15.35±0.04	15.65±0.03	14.66±0.03	14.46±0.03	14.42±0.04	14.58±0.03	0.89±0.06
	011	55245.51	15.29±0.04	15.63±0.03	14.57±0.03	14.44±0.03	14.41±0.03	14.51±0.03	0.87±0.06
	012	55273.42	15.43±0.04	15.79±0.03	14.77±0.03	14.63±0.03	14.61±0.03	14.76±0.03	0.97±0.06
	001	55291.11	15.27±0.03	15.60±0.03	14.57±0.03	14.40±0.03	14.36±0.03	14.47±0.01	0.86±0.05
90331	002	55291.18	...	...	...	14.39±0.03	...	...	...
	003	55320.09	15.20±0.03	15.47±0.03	14.39±0.03	14.20±0.03	14.16±0.03	14.28±0.03	0.74±0.08
	004	55320.26	...	...	14.39±0.02	...	...	...	...
	005	55328.85	15.17±0.03	15.42±0.03	14.38±0.03	14.21±0.03	14.18±0.03	14.29±0.03	0.79±0.07
	006	55334.20	15.16±0.03	15.46±0.03	14.40±0.03	14.22±0.03	14.18±0.03	14.29±0.03	0.79±0.07
	007	55342.14	15.15±0.03	15.42±0.02	14.37±0.03	14.17±0.03	14.13±0.03	14.29±0.03	0.79±0.08
	008	55349.50	15.22±0.03	15.51±0.03	14.45±0.03	14.25±0.03	14.25±0.03	14.35±0.03	0.79±0.08
	009	55349.75	15.24±0.03	15.49±0.02	14.39±0.03	14.27±0.03	14.23±0.03	14.30±0.03	0.79±0.09
	010	55351.08	15.18±0.03	15.45±0.02	14.39±0.03	14.22±0.03	14.17±0.03	14.29±0.03	0.78±0.07
	011	55352.81	15.19±0.03	15.46±0.02	14.37±0.03	14.39±0.01	14.18±0.03	14.42±0.03	0.88±0.12
	012	55353.15	15.18±0.03	15.42±0.02	14.39±0.03	14.25±0.03	14.16±0.03	14.30±0.03	0.80±0.08
	013	55354.60	15.18±0.03	15.45±0.02	14.41±0.03	14.21±0.03	14.19±0.03	14.31±0.03	0.79±0.08
	014	55355.20	15.18±0.03	15.45±0.02	14.38±0.03	14.20±0.03	14.15±0.03	14.27±0.03	0.76±0.07
	015	55356.73	15.16±0.03	15.43±0.02	14.36±0.03	14.17±0.03	14.12±0.03	14.27±0.03	0.76±0.08
	016	55357.62	15.19±0.04	15.46±0.02	14.39±0.03	14.18±0.03	14.13±0.03	14.25±0.03	0.72±0.08
	017	55357.24	15.17±0.03	15.40±0.02	14.37±0.03	14.18±0.03	14.12±0.03	14.25±0.03	0.75±0.07
	018	55359.55	15.17±0.03	15.40±0.02	14.38±0.03	14.19±0.03	14.17±0.03	14.28±0.03	0.80±0.07
	019	55360.48	15.17±0.03	15.45±0.02	14.38±0.03	14.25±0.03	14.16±0.03	14.28±0.03	0.78±0.07
	020	55361.52	15.15±0.03	15.41±0.02	14.34±0.03	14.17±0.03	14.12±0.03	14.22±0.03	0.75±0.07
	021	55362.59	15.14±0.03	15.40±0.02	14.32±0.03	14.12±0.03	14.07±0.03	14.16±0.03	0.68±0.06
	022	55363.73	15.11±0.03	15.38±0.02	14.32±0.03	14.11±0.03	14.05±0.03	14.17±0.02	0.72±0.07
	023	55364.65	15.14±0.03	15.37±0.02	14.31±0.03	14.09±0.03	14.02±0.03	14.15±0.03	0.69±0.06
	024	55365.78	15.11±0.03	15.36±0.02	14.30±0.03	14.10±0.03	14.01±0.03	14.13±0.03	0.69±0.07
	025	55366.81	15.11±0.03	15.35±0.02	14.29±0.03	14.09±0.03	14.04±0.03	14.15±0.03	0.72±0.07
	026	55367.89	15.11±0.03	15.36±0.02	14.30±0.03	14.11±0.03	14.05±0.03	14.18±0.03	0.72±0.08
	027	55368.85	15.16±0.03	15.38±0.02	14.33±0.03	14.12±0.03	14.10±0.03	14.19±0.03	0.72±0.07
	028	55369.65	15.12±0.03	15.38±0.02	14.34±0.03	14.15±0.03	14.10±0.03	14.23±0.03	0.77±0.07
	029	55376.40	15.11±0.03	15.36±0.02	14.31±0.03	14.10±0.03	14.08±0.03	14.18±0.03	0.75±0.07
	030	55383.74	15.09±0.03	15.35±0.02	14.30±0.03	14.10±0.03	14.05±0.05	14.17±0.03	0.75±0.07
30334	049	55384.98	...	...	14.34±0.02	...	...	...	...
90331	031	55390.19	15.18±0.03	15.44±0.03	14.39±0.03	14.21±0.03	14.19±0.03	14.29±0.02	0.79±0.07
	032	55396.22	15.17±0.03	15.41±0.02	14.33±0.03	14.18±0.03	14.12±0.03	14.25±0.03	0.75±0.09
	033	55433.79	15.25±0.03	15.48±0.02	14.44±0.03	14.29±0.03	14.26±0.03	14.34±0.03	0.79±0.07
	034	55460.69	15.34±0.03	15.61±0.02	14.61±0.03	14.42±0.03	14.40±0.03	14.51±0.03	0.84±0.06
	035	55461.66	...	...	...	...	...	14.50±0.02	...
	036	55488.39	15.38±0.03	15.62±0.02	14.63±0.03	14.45±0.03	14.43±0.03	14.53±0.03	0.84±0.06
	037	55520.15	15.42±0.03	15.74±0.02	14.76±0.03	14.61±0.03	14.64±0.03	14.77±0.03	1.00±0.07
	038	55548.29	15.40±0.03	15.70±0.02	14.71±0.03	14.54±0.03	14.53±0.03	14.68±0.03	0.93±0.07

TABLE 2—Continued

ObsID	Segment	MJD	V	B	U	UVW1	UVM2	UVW2	$\alpha_{UV}$
	039	55580.24	15.21±0.03	15.45±0.02	14.36±0.03	14.25±0.02	14.10±0.03	14.23±0.03	0.71±0.08
	040	55610.48	15.26±0.03	15.59±0.02	14.53±0.03	14.36±0.03	14.35±0.03	14.48±0.03	0.86±0.08
	041	55639.04	15.26±0.03	15.52±0.02	14.47±0.03	14.26±0.03	14.25±0.03	14.31±0.03	0.72±0.06
91017	001	55668.72	15.34±0.04	15.62±0.03	14.54±0.03	14.34±0.02	14.31±0.03	14.43±0.03	0.75±0.08
	002	55668.89	...	...	14.57±0.02	...	...	...	...
	003	55698.10	15.29±0.03	15.56±0.03	14.51±0.03	14.33±0.02	14.25±0.03	14.42±0.03	0.77±0.08
	004	55729.64	15.34±0.03	15.61±0.03	14.60±0.03	14.41±0.02	14.33±0.03	14.46±0.03	0.79±0.05
	005	55761.18	15.41±0.05	15.70±0.03	14.71±0.03	14.62±0.03	14.63±0.04	14.81±0.03	1.05±0.09
	006	55765.58	...	...	...	...	...	14.54±0.03	...
	007	55791.38	15.30±0.03	15.60±0.03	14.56±0.03	14.37±0.03	14.31±0.03	14.45±0.03	0.79±0.07
	008	55805.49	15.32±0.03	15.67±0.02	14.61±0.03	14.41±0.03	14.41±0.03	14.52±0.03	0.86±0.06
	009	55806.56	15.33±0.03	15.60±0.03	14.57±0.03	14.40±0.03	14.37±0.03	14.47±0.03	0.82±0.06
	010	55807.42	15.34±0.03	15.57±0.03	14.59±0.03	14.40±0.03	14.34±0.03	14.44±0.03	0.79±0.06
	011	55808.49	15.31±0.04	15.62±0.03	14.58±0.03	14.43±0.03	14.34±0.03	14.43±0.03	0.79±0.05
	012	55809.51	15.34±0.03	15.61±0.02	14.62±0.03	14.42±0.03	14.38±0.03	14.49±0.03	0.82±0.05
	013	55810.65	15.36±0.03	15.60±0.03	14.58±0.03	14.39±0.03	14.36±0.03	14.45±0.03	0.78±0.06
	014	55811.38	15.37±0.03	15.60±0.02	14.58±0.03	14.38±0.03	14.30±0.03	14.41±0.03	0.77±0.05
	015	55812.77	15.33±0.03	15.59±0.02	14.57±0.03	14.35±0.03	14.32±0.03	14.44±0.03	0.77±0.06
	016	55813.75	15.32±0.03	15.57±0.03	14.55±0.03	14.34±0.03	14.29±0.03	14.38±0.03	0.74±0.06
	017	55814.75	15.31±0.03	15.57±0.03	14.56±0.03	14.35±0.03	14.29±0.03	14.39±0.03	0.75±0.05
	018	55815.76	15.33±0.03	15.57±0.03	14.59±0.03	14.37±0.03	14.36±0.03	14.45±0.03	0.79±0.06
	019	55816.76	15.32±0.03	15.58±0.03	14.59±0.03	14.37±0.03	14.35±0.03	14.44±0.03	0.79±0.05
	020	55817.76	15.31±0.03	15.57±0.03	14.56±0.03	14.34±0.03	14.29±0.03	14.40±0.03	0.75±0.05
	021	55818.70	15.30±0.03	15.55±0.02	14.58±0.03	14.34±0.03	14.30±0.03	14.38±0.03	0.76±0.04
	022	55819.75	...	...	...	14.36±0.04	...	...	...
	023	55820.71	15.34±0.03	15.56±0.02	14.53±0.03	14.31±0.03	14.24±0.03	14.36±0.03	0.70±0.06
	024	55821.81	15.33±0.03	15.56±0.02	14.54±0.03	14.33±0.03	14.27±0.03	14.37±0.03	0.72±0.06
	025	55822.22	15.28±0.03	15.54±0.02	14.51±0.03	14.31±0.03	14.25±0.03	14.33±0.03	0.73±0.05
	026	55823.15	15.30±0.03	15.54±0.02	14.51±0.03	14.31±0.03	14.27±0.03	14.34±0.03	0.73±0.05
	027	55824.45	15.30±0.03	15.54±0.02	14.52±0.03	14.34±0.03	14.27±0.03	14.36±0.03	0.75±0.06
	028	55825.12	15.31±0.03	15.54±0.02	14.51±0.03	14.32±0.03	14.27±0.03	14.35±0.03	0.73±0.06
	029	55826.31	15.30±0.03	15.51±0.02	14.47±0.03	14.25±0.03	14.19±0.03	14.27±0.03	0.67±0.06
	030	55827.30	15.30±0.03	15.54±0.02	14.49±0.03	14.27±0.03	14.24±0.03	14.32±0.03	0.71±0.06
	031	55828.44	15.27±0.03	15.49±0.02	14.48±0.03	14.29±0.03	14.21±0.03	14.31±0.03	0.73±0.06
	032	55829.45	15.25±0.03	15.52±0.03	14.48±0.03	14.31±0.03	14.27±0.03	14.38±0.03	0.80±0.07
	033	55830.41	15.28±0.03	15.52±0.03	14.49±0.03	14.31±0.03	14.26±0.03	14.37±0.03	0.77±0.07
	034	55831.43	15.32±0.03	15.53±0.03	14.50±0.03	14.31±0.03	14.23±0.03	14.36±0.03	0.72±0.07
	035	55832.89	15.30±0.03	15.56±0.03	14.52±0.03	14.37±0.03	14.30±0.03	14.42±0.03	0.81±0.07
	036	55833.08	15.29±0.03	15.56±0.03	14.53±0.03	14.35±0.03	14.28±0.03	14.41±0.03	0.79±0.06
	037	55834.51	15.31±0.03	15.57±0.02	14.56±0.03	14.38±0.03	14.34±0.03	14.46±0.03	0.82±0.06
	038	55852.41	15.28±0.03	15.54±0.02	14.55±0.03	14.33±0.03	14.27±0.03	14.34±0.03	0.75±0.04
	039	55882.65	15.32±0.03	15.53±0.02	14.52±0.03	14.32±0.03	14.30±0.03	14.41±0.03	0.78±0.07
	040	55912.29	15.25±0.03	15.51±0.02	14.47±0.03	14.31±0.03	14.29±0.03	14.44±0.03	0.85±0.09
	041	55943.52	15.39±0.04	15.70±0.03	14.71±0.03	14.57±0.03	14.51±0.03	14.72±0.03	0.96±0.08
	042	55946.46	15.39±0.03	15.71±0.03	14.70±0.03	14.58±0.03	14.56±0.03	14.68±0.03	0.95±0.06
	043	55974.50	15.41±0.03	15.73±0.02	14.76±0.03	14.61±0.02	14.58±0.03	14.75±0.03	1.00±0.06
	044	56003.31	15.41±0.03	15.71±0.02	14.75±0.03	14.61±0.03	14.61±0.03	14.77±0.03	1.02±0.07
30334	050	56038.31	...	...	...	...	14.53±0.03	...	...
	051	56066.75	...	...	...	...	14.66±0.03	...	...
	052	56094.62	...	...	...	...	14.73±0.03	...	...
	053	56122.79	...	...	...	...	14.66±0.03	...	...
	054	56150.44	...	...	...	...	14.48±0.03	...	...
	055	56178.30	...	...	...	...	14.33±0.03	...	...
	056	56206.89	...	...	...	...	14.55±0.03	...	...
	057	56234.48	...	...	...	...	14.54±0.03	...	...
	058	56262.38	...	...	...	...	14.74±0.03	...	...
	059	56290.59	...	...	...	...	14.75±0.03	...	...
	060	56318.18	...	...	...	...	14.58±0.03	...	...
	062	56350.30	...	...	...	...	14.60±0.03	...	...
	063	56374.49	...	...	...	...	14.66±0.03	...	...
	064	56402.12	...	...	...	...	14.72±0.03	...	...
	065	56430.08	...	...	...	...	14.70±0.03	...	...
	066	56444.77	15.47±0.04	15.80±0.03	14.87±0.03	14.83±0.03	14.79±0.03	14.96±0.03	...
	067	56445.92	15.45±0.04	15.80±0.03	14.92±0.03	14.84±0.03	14.82±0.03	14.98±0.03	...
	068	56446.69	15.53±0.04	15.86±0.03	14.87±0.03	14.80±0.03	14.81±0.03	15.00±0.03	...
	069	56447.85	15.49±0.04	15.82±0.03	14.96±0.03	14.89±0.03	14.85±0.03	14.99±0.03	...
	070	56448.53	15.57±0.05	15.84±0.03	14.89±0.03	14.83±0.03	14.80±0.03	14.97±0.03	...
	071	56449.63	15.53±0.04	15.84±0.03	14.96±0.03	14.86±0.03	14.91±0.03	15.04±0.03	...
	072	56450.40	15.48±0.06	15.81±0.03	14.92±0.03	14.81±0.03	14.89±0.08	14.97±0.03	...
	073	56451.53	15.54±0.04	15.86±0.03	14.92±0.03	14.81±0.03	14.83±0.03	14.97±0.03	...
	074	56452.87	15.52±0.05	15.83±0.03	14.87±0.03	14.78±0.03	14.77±0.04	14.96±0.03	...
	075	56453.93	15.49±0.04	15.87±0.03	14.91±0.03	14.78±0.04	14.84±0.04	14.98±0.03	...
	076	56458.54	...	...	...	...	14.85±0.03	...	...
	077	56486.48	...	...	...	...	14.83±0.03	...	...

<sup>1</sup>Magnitude corrected for reddening with  $E_{B-V}=0.037$  given by Schlegel et al. (1998). The errors given in this table are statistical errors

TABLE 3  
*Swift* XRT  $3\sigma$  UPPER LIMITS OF WPVS 007

ObsID	Segment	MJD	$3\sigma$ ul		
30334	015	54299.81	4.54		
	018	54349.96	2.42		
	021	54354.52	2.25		
	022	54355.53	1.82		
	023	54356.52	1.68		
	024	54357.52	1.52		
	026	54380.30	3.43		
	027	54381.31	2.54		
	028	54413.06	2.54		
	029	54449.70	4.26		
	030	54477.85	5.04		
	031	54636.14	1.54		
	032	54666.69	2.70		
	033	54694.18	3.11		
	034	54730.45	10.06		
	035	54742.67	3.74		
	036	54756.69	17.49		
	037	54760.27	2.12		
	038	54793.10	3.34		
	040	54827.09	2.02		
	041	54828.16	5.34		
	043	54847.08	2.87		
	044	54881.95	5.27		
	045	54887.64	1.04		
	046	54909.85	2.71		
	047	54937.03	4.88		
	90108	048	54972.88	2.47	
		001	55000.90	2.71	
		002	55031.80	3.00	
		004	55062.07	4.52	
		006	55097.15	2.53	
		007	55119.83	4.15	
		008	55154.85	2.07	
		009	55182.35	4.30	
		010	55217.06	6.01	
		011	55245.51	2.88	
		012	55273.42	2.89	
		90331	001	55291.11	2.68
			002	55291.18	3.42
	003		55320.09	2.45	
	004		55320.26	3.76	
	005		55328.85	1.39	
	006		55334.20	2.87	
	007		55342.14	1.17	
	008		55349.50	2.13	
	009		55349.75	1.78	
	010		55351.08	2.45	
011	55352.81		2.61		
012	55353.15		1.55		
013	55354.60		1.12		
014	55355.20		7.54		
015	55356.73		1.89		
016	55357.62		2.09		
017	55357.24		2.16		
018	55359.55		1.54		
019	55360.48		1.37		
020	55361.52		2.35		
022	55363.73		1.18		
023	55364.65		1.32		
024	55365.78		2.02		
025	55366.81		1.88		
026	55367.89		2.12		
027	55368.85		4.76		
029	55376.40		1.35		
032	55396.22		1.45		
033	55433.79		1.77		
035	55461.66		6.58		
036	55488.39		1.76		
037	55520.15		1.97		
038	55548.29		1.45		
039	55580.24	1.63			
040	55610.48	3.28			
041	55639.04	1.86			
91017	001	55668.72	2.45		
	002	55668.89	3.51		
	003	55698.10	2.16		
	004	55729.64	2.59		
	005	55761.18	8.63		
	007	55791.38	2.28		
	009	55806.56	4.63		
	010	55807.42	1.59		
	011	55808.49	4.90		
	012	55809.51	1.61		
	013	55810.65	2.78		
	014	55811.38	3.00		
	015	55812.77	3.06		



TABLE 3—*Continued*

ObsID	Segment	MJD	$3\sigma$ ul
	016	55813.75	3.32
	017	55814.75	3.60
	019	55816.76	2.51
	020	55817.76	2.16
	021	55818.70	2.40
	023	55820.71	3.23
	024	55821.81	1.68
	026	55823.15	2.42
	027	55824.45	2.18
	028	55825.12	4.56
	029	55826.31	3.47
	032	55829.45	2.73
	033	55830.41	2.34
	034	55831.43	1.95
	035	55832.89	2.96
	036	55833.08	3.74
	037	55834.51	1.77
	038	55852.41	1.95
	039	55882.65	2.88
	040	55912.29	1.68
	041	55943.52	3.71
	042	55946.46	1.36
	043	55974.50	1.11
	044	56003.31	2.03
30334	050	56038.31	3.11
	051	56066.75	3.49
	052	56094.62	4.61
	053	56122.79	3.00
	054	56150.44	4.03
	055	56178.30	5.16
	056	56206.89	3.83
	057	56234.48	3.08
	058	56262.38	2.98
	059	56290.59	2.45
	060	56318.18	3.02
	062	56350.30	3.87
	063	56374.49	4.88
	064	56402.12	2.95
	065	56430.08	3.25
	066	56444.77	5.74
	067	56445.92	5.27
	068	56446.69	2.34
	069	56447.85	4.04
	070	56448.53	3.05
	071	56449.63	4.80
	072	56450.40	4.39
	073	56451.53	2.99
	074	56452.87	3.82
	075	56453.93	4.75
	076	56458.54	2.93
	077	56486.48	3.08

<sup>1</sup>The  $3\sigma$  upper limits are calculated using the method by Kraft et al. (1991) and are given in units of  $10^{-3}$  counts  $s^{-1}$ .

TABLE 4  
DETECTION OF WPVS 007 BY *Swift*

Obs date	$T_{\text{exp}}^1$	Source counts <sup>2</sup>	CR <sup>3</sup>	HR <sup>4</sup>	0.2-2.0 keV flux <sup>5</sup>	$\alpha_{\text{ox}}^6$
2007 September	50531	$30.0^{+6.0}_{-5.2}$	$5.9^{+1.2}_{-1.0}$	$+0.54^{+0.18}_{-0.12}$	$1.48 \pm 0.33$	—
2008 December 21	2330	$9.7^{+3.5}_{-2.9}$	$41.2^{+15.0}_{-12.5}$	—	$17.55^{+6.39}_{-5.33}$	1.95
2009 September 17	1818	$33.3^{+6.3}_{-5.5}$	$183.2^{+34.6}_{-30.3}$	$-0.54^{+0.13}_{-0.16}$	$160.0^{+30.2}_{-26.5}$	1.89
2010 June 15	5020	$6.2^{+3.0}_{-2.3}$	$12.4^{+6.0}_{-4.6}$	—	$5.28^{+2.56}_{-1.96}$	2.38
2010 June 22	4848	$6.3^{+3.1}_{-2.3}$	$13.0^{+6.4}_{-4.7}$	—	$5.54^{+2.73}_{-2.00}$	2.36
2010 July 06	5218	$17.9^{+4.8}_{-4.1}$	$34.3^{+9.2}_{-7.9}$	$-0.48^{+0.20}_{-0.25}$	$22.76^{+6.12}_{-5.24}$	2.36
2010 July 13	4111	$40.6^{+6.8}_{-6.1}$	$98.8^{+16.5}_{-14.8}$	$-0.11^{+0.14}_{-0.16}$	$53.4^{+8.9}_{-8.0}$	1.87
2010 September 21	3516	$17.2^{+4.6}_{-3.9}$	$48.9^{+13.1}_{-11.1}$	$-0.25^{+0.11}_{-0.15}$	$22.66^{+6.07}_{-5.14}$	2.28
2011 July 23	4750	$25.1^{+5.6}_{-4.9}$	$52.8^{+12.1}_{-10.3}$	$-0.05^{+0.19}_{-0.22}$	$37.56^{+8.61}_{-7.3}$	2.07
2011 September 01	5377	$8.4^{+3.5}_{-2.9}$	$15.6^{+6.5}_{-5.4}$	—	$4.22^{+1.76}_{-1.46}$	2.75
2011 September 11	5032	$10.0^{+3.8}_{-3.1}$	$19.9^{+7.6}_{-6.2}$	—	$5.38^{+2.05}_{-1.68}$	2.67
2011 September 18	5201	$10.2^{+4.2}_{-3.6}$	$19.6^{+8.1}_{-6.9}$	—	$5.29^{+2.19}_{-1.87}$	2.35
2011 September 23	4650	$12.0^{+4.1}_{-3.4}$	$25.8^{+8.8}_{-7.3}$	—	$6.97^{+2.38}_{-1.97}$	2.31
2011 September 24	4860	$8.7^{+3.7}_{-3.0}$	$17.9^{+7.6}_{-6.2}$	—	$4.84^{+2.05}_{-1.68}$	2.62
2011 September <sup>9</sup>	25220	$49.2^{+8.2}_{-7.5}$	$19.5^{+3.3}_{-3.0}$	$+0.24 \pm 0.16$	$5.27^{+0.89}_{-0.81}$	—

<sup>1</sup>Exposure times are given in s

<sup>2</sup>Source counts are background corrected and the uncertainties were determined using Bayesian statistics as described in Kraft et al. (1991).

<sup>3</sup>Count rate is given in units of  $10^{-4}$  counts  $\text{s}^{-1}$ .

<sup>4</sup>The hardness ratio is defined as  $\text{HR}=(\text{H}-\text{S})/(\text{H}+\text{S})$  with S and H are background subtracted counts in the 0.3-1.0 and 1.0-10.0 keV bands, respectively. The hardness ratio was calculated following the description in Park et al. (2006).

<sup>5</sup>The rest-frame 0.2-2.0 keV flux is given in units of  $10^{-17}$   $\text{W m}^{-2}$ , corrected for Galactic absorption

<sup>6</sup>Observed  $\alpha_{\text{ox}}$ ; the uncertainties in  $\alpha_{\text{ox}}$  are of the order of 0.2.

<sup>7</sup>Assuming the X-ray spectrum measured during the 2010 July 13 *Swift* observation.

<sup>8</sup>Assuming the mean X-ray spectrum of the 2011 September *Swift* observations.

<sup>9</sup>Mean values of all data when WPVS 007 was detected during the 2011 September intensive monitoring campaign.

TABLE 5  
SPECTRAL ANALYSIS OF WPVS 007 DURING DETECTIONS<sup>1</sup>

Obs date	Model <sup>2</sup>	$\alpha_X$	$N_{H,pc}$ <sup>3</sup>	$f_{pc}$ <sup>4</sup>	C-stat
2007 September	powl	$-0.84^{+0.57}_{-0.88}$	—	—	50.3/40
	zpcfabs * po	$0.77^{+0.44}_{-0.51}$	$13.73^{+13.86}_{-6.87}$	0.95	42.6/39
2009 September 17	powl	$2.67^{+0.76}_{-0.65}$	—	—	20.6/26
	zpcfabs	$2.65^{+1.00}_{-0.67}$	$17.39^{+137.83}_{-8.58}$	0.95	17.6/25
2010 July 13	powl	$1.56^{+0.47}_{-0.45}$	—	—	36.1/32
	zpcfabs	$2.76^{+0.50}_{-1.34}$	$2.80^{+62.50}_{-1.37}$	0.95	32.1/31
2011 July 23	powl	$1.66^{+0.70}_{-0.61}$	—	—	34.4/20
	zpcfabs	$2.83^{+0.54}_{-0.56}$	$3.02^{+3.88}_{-1.40}$	0.95	24.1/19
2011 September <sup>5</sup>	powl	$-0.40^{+0.84}_{-1.06}$	—	—	48.9/25
	zpcfabs	$1.73^{+0.42}_{-0.42}$	$8.45^{+5.65}_{-2.40}$	0.95	28.5/24
2005-2013 <sup>6</sup>	powl	+0.24	—	—	30.5/12
	zpcfabs	$0.91^{+0.32}_{-0.35}$	$22.3^{+19.4}_{-9.5}$	$0.909^{+0.053}_{-0.107}$	134/180

<sup>1</sup>All spectra were fitted with the z=0 absorber fixed to the Galactic value of  $N_H = 1.4 \times 10^{20}$  cm<sup>-2</sup>.

<sup>2</sup>powl = single power law model, zpcfabs \* powl = partial covering absorber with single power law model

<sup>3</sup>The partial covering absorber column density  $N_{H,pc}$  is given in units of  $10^{22}$  cm<sup>-2</sup>

<sup>4</sup>Covering fraction of the partial covering absorber

<sup>5</sup>Mean spectrum of all data when WPVS 007 was detected during the 2011 September intensive monitoring campaign.

<sup>6</sup>Mean spectrum of all data when WPVS 007 was not detected between October 2005 and June 2013 as listed in Table 3.

TABLE 6  
INFRARED OBSERVATIONS OF WPVS 007 WITH 2MASS AND WISE.

Filter	$\nu_c$ <sup>1</sup>	Flux <sup>2</sup>	$\nu L_\nu$ <sup>3</sup>
2MASS J	2.40	$1.7568 \pm 0.10656$	2.94
2MASS H	1.82	$1.4888 \pm 0.12867$	2.49
2MASS K	1.38	$1.5456 \pm 0.095634$	2.59
WISE 3.4 $\mu$	0.8856	$1.5428 \pm 0.030132$	2.58
WISE 4.6 $\mu$	0.6445	$1.4232 \pm 0.025126$	2.38
WISE 12 $\mu$	0.2675	$1.2072 \pm 0.016795$	2.02
WISE 22 $\mu$	0.1346	$1.2472 \pm 0.029052$	2.09

<sup>1</sup>Central filter frequency  $\nu_c$  in units of  $10^{14}$  Hz

<sup>2</sup>Flux  $\nu F_\nu$  and flux uncertainty are given in units of  $10^{-14}$  W m<sup>-2</sup>

<sup>3</sup>The luminosity  $\nu L_\nu$  is given in units of  $10^{36}$  W.

TABLE 7  
NIR EMISSION LINES IN WPVS 007.

Line	$\lambda_0^1$	FWHM <sup>2</sup>	Flux <sup>3</sup>
Mg II	9218+9244	—	43.8
FeII + Pa $\epsilon$	9549 + 9573	—	20.7
Fe II	9997	1680	15.5 $\pm$ 3.8
Pa $\delta$	10052	1310	16.5 $\pm$ 3.4
Fe II	10501	1570	10.6 $\pm$ 0.9
He I	10833	1490	43.3 $\pm$ 4.5
Pa $\gamma$	10941	1730	34.7 $\pm$ 5.0
Fe II	11126	1070	4.7 $\pm$ 0.9
O I	11290	1320	18.0 $\pm$ 1.7
O III	12470	990	5.3 $\pm$ 0.7
Fe II	12570	1300	4.2 $\pm$ 0.9
Pa $\beta$	12822	1230	39.3 $\pm$ 3.2
O III	13436	885	13.8 $\pm$ 2.0
Fe I	14298	—	—
Fe I	14480	—	—
Fe I	14628	—	—
Fe I	15260	—	—
Fe I	15335	—	—
Fe I	15463	—	—
Fe I	15533	—	—
Fe I	15680	—	—
Fe I	15956	—	—
Fe I	16366	—	—
Fe I	16445	—	—
Fe I	16885	—	—
Fe I	17383	—	—
Fe I	17675	—	—
Pa $\alpha$	18751	1035	53.4 $\pm$ 5.6
He I	18922	1400	11.0 $\pm$ 1.3
Br $\delta$	19400	—	—
Mg II	21064	775	4.9 $\pm$ 0.6
Br $\gamma$	21661	1130	6.5 $\pm$ 0.7

<sup>1</sup>Rest wavelength  $\lambda_0$  given in units of Å

<sup>2</sup>Full Width at Half Maximum (FWHM) given in units of km s<sup>-1</sup>. Note that for the FeI lines FWHM and flux can not be given reliably because these lines appear to be blended and often so faint that they are affected by noise.

<sup>3</sup>The Line flux  $\nu F_\nu$  and flux uncertainty given in units of 10<sup>-18</sup> W m<sup>-2</sup> (10<sup>-15</sup> erg s<sup>-1</sup> cm<sup>-2</sup>).